A LABORATORY INVESTIGATION OF FREE SURFACE FLOWS OVER WAVY BEDS

by

Albert F. H. Yuen and John F. Kennedy

Sponsored by
United States Department of the Interior
U.S. Geological Survey
Contract No. 14-08-0001-11420

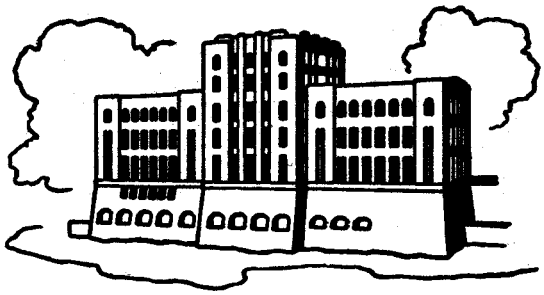

IIHR Report No. 121

Iowa Institute of Hydraulic Research
The University of Iowa
Iowa City, Iowa

December 1971

A LABORATORY INVESTIGATION OF FREE SURFACE FLOWS OVER WAVY BEDS

by

Albert F. H. Yuen and John F. Kennedy

Sponsored by
United States Department of the Interior
U.S. Geological Survey
Contract No. 14-08-0001-11420

IIHR Report No. 121

Iowa Institute of Hydraulic Research
The University of Iowa
Iowa City, Iowa

December 1971

ABSTRACT

The primary goal of the experimental investigation reported herein was to verify the linearized, third-order analytical model developed by Iwasa and Kennedy (1968) to predict the amplitude ratio and phase shift between bed and surface waves of free-surface flows over sinusoidal beds. The agreement between experimental and theoretical results is found to be quite good, except near the resonance point (which occurs at approximately the flow velocity equal to the celerity of a small-amplitude surface wave, in a fluid with the mean flow depth); near resonance the surface configuration is complicated by the formation of a hydraulic jump over each bed wave, and can only be analyzed within the framework of a nonlinear model. For selected experiments the spatial distributions of velocity, total head, bed pressure, and bed shear stress were also measured. The effects of bed curvature on the distributions of these quantities are discussed in the light of the findings of Hsu and Kennedy's investigation of flow in wavy-walled pipes. The form of the velocity distribution was found to vary widely along each wave, but to conform over much of the depth to the power law; an expression for the exponent in the velocity distribution relation is derived from energy and continuity considerations.

ACKNOWLEDGEMENT

The authors gratefully acknowledge the assistance of Dr. Touvia Miloh of The Iowa Institute of Hydraulic Research in checking the data and manuscript and in bringing the report to completion.

TABLE OF CONTENTS

LIST OF FIGURES

LIST OF FIGURES
(continued)

LIST OF FIGURES
(continued)

LIST OF TABLES

A LABORATORY INVESTIGATION OF FREE SURFACE FLOWS OVER WAVY BEDS

I. INTRODUCTION

A. Introductory Remarks. Real-fluid flows past boundaries of regular periodic form have attracted considerable interest in recent years because of the important role they play in several natural phenomena, including generation of water waves by wind, the formation of cave flutes on limestone surfaces by flows of fluids that dissolve the boundary material, the growth of ice ripples on the underside of river ice-covers, and the production of aeolian and aqueous sediment ripples. Moreover, this class of flows is of considerable interest in its own right because of the nonuniform distortion it produces in the turbulence field, and of the effects on the boundary layer of the alternate convergence and divergence of the flow and the periodically nonuniform curvature of the boundary.

The purpose of the primarily experimental investigation reported herein was to verify the principal results of the third-order linearized analytical model developed by Iwasa and Kennedy (1968) for free surface shear flows over wavy beds. Flume experiments were conducted using two different sinusoidal-profile beds. Free-surface profiles were measured in all experiments, and distributions of wavy-boundary shear stress and pressure, mean velocity, and total head were measured in selected runs. In Chapter II a description of the experimental apparatus and techniques is presented, Chapter III reports and interprets the results, and Chapter IV summarizes the principal conclusions.

B. Previous Related Investigations. In this section a brief, summary review of earlier related work will be presented. Lamb (1932) and Milne-Thomson (1960) recount the linearized potential-flow analysis of free surface flow over a rigid sinusoidal bed of small steepness. The principal results of that calculation is an expression for amplitude of the surface wave and the prediction that the bed and surface waves are in phase or π out of phase according as

$$U^2 \gtrless \frac{g}{k} \tanh kd \qquad (1)$$

where U is the mean velocity, $k = 2\pi/L$ is the wave number, L is the wavelength of the bed, and d is the mean depth.

Stanton, Marshall, and Houghton (1932), Motzfeld (1937), and Gupta and Mollo-Christensen (1966) conducted wind tunnel tests on flows over wavy beds, to measure the pressure distribution and the boundary layer development along the bed and the mean-velocity distribution in the flow. The first two of these investigations have been discussed in some detail by Brooke-Benjamin (1959) in the introductory remarks preceding his theoretical analysis of semi-infinite shear flows over a two-dimensional wavy boundary; his analytical model predicts an upstream phase shift of $\pi/6$ of the boundary shear stress and boundary pressure relative to the bed wave. Hsu and Kennedy (1971) obtained detailed measurements of the distributions of mean velocity, pressure, total head, boundary shear stress, turbulence intensities, and Reynolds stresses for flows in two different circular-cross-section pipes with diameters that varied sinusoidally along their lengths. They found that the boundary shear stress is shifted upstream relative to the wall profile, the mean-velocity profiles undergo wide variation along each wave, and the turbulence intensity over a central core occupying some sixty percent of the radius is constant along the pipe. Sigal (1971) made measurements comparable to those of Hsu and Kennedy (1971) in low-speed flows over two different two-dimensional sinusoidal beds in a wind tunnel, with essentially similar findings. He found that the boundary curvature modulates the slope of the semi-logarithmic portion of the velocity profiles and renders the law of the wake invalid. However, the total velocity (the stagnation pressure) was found to obey the law of the wake, and mixing length and eddy viscosity profiles based on the derivative of the total velocity were found to be unaltered by the boundary waviness.

The linearized potential-flow formulation of free-surface wavy-bed flow contains a singularity (predicted infinite surface wave amplitude) at the resonant velocity; i.e., at the flow velocity, given by the right side of (1), equal to the celerity of a small-amplitude wave on a liquid with undisturbed depth equal to the mean flow depth. Mei (1969) analyzed the resonance speed to the second order of approximation in surface amplitude using a potential-flow analysis and Lindstedt's method for nonlinear oscillations goverened by ordinary differential equations. He demonstrated that the predicted free surface amplitude always remains finite when the nonlinearity of the problem

is taken into account, and obtained curves relating the surface amplitude to the depth and velocity of flow and the amplitude and wavelength of the sinusoidal bed. Nielsen (1970) formulated a second-order approximation to the stream-function formulation of free-surface shear flow over a wavy bed. Much of his effort was directed toward obtaining numerical solutions to the resulting boundary value problem. He found that except near the resonant Froude number the second-roder results do not differ significantly from those of the first-order formulation. The principal advantages of the second-order analysis are that it permits the form drag on the bed waves to be taken into account, and gives a better approximation to the actual shapes of the surface waves.

Vincenti (1959) and Rhyming (1963) analyzed wavy-boundary flows of gases in chemical or vibrational nonequilibrium. Robillard and Kennedy (1967) presented the results of a flume study similar to that reported herein and described the various free-surface configurations that occur. Much of their investigation was concerned with the diagonal "shock" waves formed in supercritical wavy-bed flows by the interaction between the boundary layers of the flume walls and the centrifugally induced secondary currents.

Since one of the primary goals of the present study was to verify the results of Iwasa and Kennedy's (1968) analysis of free-surface shear flow, it is in order to summarize their principal results here. Let the bed profile $\delta(x)$, be given by

$$\delta(x) = \delta_o \sin kx \tag{2}$$

and the depth variation in the streamwise direction by

$$\eta(x) = \eta_o \sin(kx + \phi) \tag{3}$$

where δ_o and η_o are the amplitudes of the bed wave and depth wave, respectively. Iwasa and Kennedy's third-order linearized analysis yielded the following expressions for the normalized depth-variation amplitude, η_o/δ_o, and the phase shift, ϕ:

$$\frac{\eta_o}{\delta_o} = \frac{\mu\sqrt{(1-\lambda_1\mu^2F^2)^2 + \frac{\mu^2f^2F^4}{64}}}{\sqrt{\mu^2[(\alpha_1 + \lambda_2\mu^2)F^2-1]^2 + \frac{9f^2F^4}{64}}} \tag{4}$$

where $\mu = 2\pi d/L$, $F^2 = U^2/gd$, f is the Darcy-Weisbach friction factor, λ_1 and λ_2 are the Jaiger coefficients ($\lambda_1 = 1/2$ and $\lambda_2 = 1/3$ for flows with uniform velocity distribution over beds of small curvature), and α_1 is the Coriolis (energy flux) coefficient; and

$$\tan \phi = -\frac{fF^2}{8\mu} \frac{\{3+\mu^2[(\alpha_1 - 3\lambda_1)F^2-1] + \lambda_2\mu^4F^2\}}{\{[(\alpha_1+\lambda_2\mu^2)F^2-1]\ [\lambda_1\mu^2F^2-1] + \frac{3f^2F^4}{64}\}} \qquad (5)$$

Expressions similar to these have been derived by Engelund and Hansen (1966) from a calculation comparable to the linearized analysis of Iwasa and Kennedy (1968). Equations (4) and (5) constitute the main analytical framework for examination of the experimental results obtained in the present investigation. The relations between F and the quantities η_o/δ_o and ϕ given by (4) and (5) are presented graphically in Chapter III. Iwasa and Kennedy present a thoroughgoing analysis and discussion of the variations of η_o/δ_o and ϕ with F for different relations among μ, λ_1, λ_2, and α_1. They also analyzed the second-order, nonlinear formulation, and calculated several water-surface profiles to illustrate the principal different types of behavior.

II. APPARATUS AND PROCEDURE

All experiments reported herein were conducted in a glass-walled, tilting laboratory flume with a channel that is 85 feet long, 2.5 feet wide, and 10 inches deep. The water flow was supplied by the laboratory constant-head system, and discharge was measured by means of a point gage and a V-notch weir located in the head tank of the flume. Bed and water surface elevations were measured with a point gage with resolution of 0.001 foot mounted on a carriage which rides on the stainless steel rails attached to the tops of the flume walls. Channel slope was determined from a counter activated through gears by one of the jack screws which support the flume channel.

Two different bed geometries were investigated. Both beds had sinusoidal longitudinal profiles and extended across the full width of the flume. Their geometrical characteristics are summarized in table 1.

Table 1

Geometry of Wavy Beds

	No. of Waves	Wave-length (ft.)	Amplitude (δ^o)
Bed I :	15	1.00	0.034
Bed II:	10	1.50	0.023

The wavy beds were fabricated by attaching aluminum sheet to three longitudinal stringers which were contoured to the desired profile and secured in the flume. The surfaces of the beds were hydrodynamically smooth. The beds commenced and ended at wave troughs, to provide continuous transitions with the flume floor. The upstream end of each test bed was positioned immediately downstream from the tilting diffuser gate at the channel inlet, so that the flow entering upon the waves had a fairly uniform velocity distribution and, more importantly, was free from the stationary surface waves which inevitably occur at Froude numbers greater than about 0.5 to 0.6.

Velocity head, total head, and piezometric head were measured using a 0.125-inch diameter Prandtl tube and a two-tube air-water manometer with 0.001-foot resolution. At each measurement section along the bed the probe was inclined so that the sensor leg was parallel with the mean flow direction at that station; for flows in which the bed and surface waves were in phase the probe was nearly parallel with the bed, while for low velocity flows with bed and surface waves out of phase the probe inclination was midway between the local bed and surface slopes. The deviation between the local velocity direction and the probe axis was always less than 10°. Boundary shear stress was determined by means of a modified Preston tube (*Zweilochsonde*) of the type described by Rechenberg, Schwefel, and Bienert (1967); the probe was fabricated from 1.0 mm hypodermic tubing, which has sufficient flexibility that end of the sensor could be made tangent to the undulating bed at any station. The probe used is described in detail and illustrated in a sketch in a recent paper by Hsu and Kennedy (1971). The probe was calibrated in steady, uniform free-surface flows, and the head difference (total head minus static head) between its two elements was measured with a differential air-water manometer. Piezometric head on the wavy beds was measured with a multi-tube manometer through 0.0625-inch piezometers installed along the second and third waves from the

upstream ends of the test sections at intervals of $\pi/4$ and $\pi/10$ on Beds I and II, respectively. Each piezometer was offset 0.75 inch laterally from the adjacent upstream one to eliminate any interference effects between piezometers.

In each experiment the required discharge was established and the openings of the flume inlet diffuser gate and/or outlet weir and the flume slope were adjusted as required to produce quasi-uniform flow with the desired mean depth over the wavy bed. Water-surface profiles were then measured along the center plane of the flume over a section beginning at the crest of the second or third wave downstream from the upstream end of the bed and extending downstream over two or more waves, or to the intersection of the first two shock waves (see Robillard and Kennedy, 1967, for a thoroughgoing discussion of these shock waves). The other quantities of interest were then measured; the spatial intervals between measurements can be determined from the numerous data plots presented in the next chapter.

III. PRESENTATION AND DISCUSSION OF RESULTS

Tables 2 and 3 present summaries of the results obtained from the experiments with Beds I and II, respectively. The mean (along the measurement section) depth, d; mean velocity, U; nondimensional wave number, $\mu = 2\pi d/L$; Froude number, $F = U^2/gd$; and mean shear stress were all calculated directly from the measured discharge, bed and water surface profiles, and flume slope, and the known values of the flume width and bed wavelengths. The other data included in tables 2 and 3 are concerned with the magnitudes and phase shifts (relative to the bed waves) of the spatially periodic undulations in the streamwise direction of the water surface elevation (surface wave), depth (depth wave), bed pressure-head (pressure wave), and bed shear stress (shear wave). All quantities were not determined in every experiment, as is evident from tables 2 and 3; in many runs only water surface profiles were measured. Those runs which produced a hydraulic jump over each wave, of the type described by Robillard and Kennedy (1967) and analyzed by Iwasa and Kennedy (1968), are indicated under the Remarks column in the tables. In most cases the streamwise variations of the spatially periodic quantities were nearly sinusoidal. For all cases the amplitude reported is half of the average difference between the maxima and the minima of the quantity, and the phase shift is the average of the phase distance between

the crests and troughs of the bed waves and the adjacent maxima and minima, respectively, of the quantity being examined. In the ensuing sections the experimental data are presented and discussed in some detail.

A. Free Surface Waves. Figures 1A through 1R present measured water surface elevation, E, the local depth, $D = d + \eta(x)$, calculated therefrom, and the distribution of the normalized local bed shear stress $2\tau_o/\rho U^2$ for 18 experiments with Bed II. These figures give an idea of the forms of the distributions of these quantities for a range of conditions and permit the reader to gain an idea of the accuracy and significance of the amplitude ratios and phase shifts reported in tables 2 and 3.

Note in figures 1A through 1R that for flows at the higher Froude numbers, the depth is nearly constant; see, for example, figures 1J, 1K, 1M, 1N, and 1O. In these cases the depth wave is so small that it is not possible to use it to verify (4) and (5), but the free surface wave is readily measureable. On the other hand, at lower Froude numbers the water surface is so nearly flat (refer, for example, to Runs 112, 136, and 137 in table 2) that the surface wave was not readily discernible but the depth wave could be determined accurately. Hence to verify the analytical model developed by Iwasa and Kennedy, it is desirable to have expressions for the amplitude ratio and phase shift of the surface wave, to complement the corresponding relations, (4) and (5), for the depth wave.

If the bed profile is given by (2) and the depth wave by (3), (4), and (5), it can readily be shown that the water surface elevation, $\xi(x)$, is given by

$$\xi(x) = \xi_o \sin(kx + \theta) \tag{6}$$

where

$$\xi_o/\delta_o = \sqrt{1 + (\eta_o/\delta_o)^2 + 2(\eta_o/\delta_o)\cos\phi} \tag{7}$$

and

$$\tan\theta = \frac{\eta_o}{\delta_o}\,\frac{\sin\phi}{1 + (\eta_o/\delta_o)\cos\phi} \tag{8}$$

Figures 2C through 2E present a comparison between the measured amplitude ratios and phase shifts for the surface and depth waves and those given by (4), (5), (7), and (8), using $f = 0.02$, $\lambda_1 = 1/2$, $\lambda_2 = 1/3$, and

$\alpha_1 = 1$. From these figures it can readily be appreciated why it is necessary to consider both surface and depth waves to verify the analytical results. Over ranges of F where the depth wave is so small as to be not readily measured (e.g., F greater than about 1.2 for $\mu = 0.7$, the case depicted in figure 2A), thus making determination of ϕ nearly impossible, the surface wave is easily defined ($\xi_o/\delta_o \simeq 1$) and θ can be measured with a relatively high degree of accuracy. Similarly, where $\xi_o \simeq 0$ ($F \lesssim 0.5$ for $\mu = 0.7$; figure 2A) and θ cannot be measured accurately, $\eta_o/\delta_o \simeq 1$ and θ easily can be determined. This consideration accounts for not all phase-shift points being shown on both graphs in each of figures 2A through 2E.

The correspondence between theoretical and experimental results is remarkably good, especially when it is considered that the analytical model is derived from a linearization of a third-order approximation to the complete one-dimensional energy formulation. Note in particular that as ϕ changes, with increasing F, from π to nearly 0 or 2π and then back to π, the transition occurs through phase shifts $0 < \phi < \pi$, rather than through $\pi < \phi < 2\pi$. The uncertainty about the path of the transition in ϕ from π back to π originates from questions concerning how the governing equation should be linearized. This point is treated at length in the discussion by Hansen (1969) and the discussion closure by Iwasa and Kennedy (1970) of Iwasa and Kennedy's (1968) theoretical paper on wavy-bed flow. The physical aspect of this question is as follows. At very low Froude numbers the surface and bed waves are π out of phase. With increasing F the surface wave shifts until it is nearly in phase with the bed wave at large F. Whether this transition occurs by the surface wave moving upstream or downstream determines if the transition in ϕ takes place through 0 or 2π. The theory of Kennedy and Iwasa (1968) and the data of figures 2A through 2E indicate that the surface wave movement is upstream for the values of μ examined ($\mu \lesssim \sqrt{6}$). It should be noted, however, that for μ greater than that for which the numerator and denominator of (4), with friction-factor terms neglected, are equal, i.e., for $\mu > \mu_c$ where

$$\mu_c = \sqrt{\frac{\alpha_1}{\lambda_1 - \lambda_2}} \qquad (9)$$

the transition occurs by the waves moving downstream; i.e., through $\pi < \phi < 2\pi$.

It is not possible, regrettably, to obtain surface-profile data near the "resonant" point; i.e., over the range of F where η_o and ξ_o become very large. For these Froude numbers a hydraulic jump forms over the trough or on the upstream slope of each bed wave. Experiments in which these jumps formed are indicated in tables 2 and 3. This phenomenon is described by Robillard (1965) and by Robillard and Kennedy (1967), and is analyzed by Iwasa and Kennedy (1968). Formation of these jumps is probably responsible for the breaking of stationary waves that form above antidunes. The antidunes increase in amplitude until the streamwise momentum balance of the flow can be ahcieved in either of two modes: in flow with jumps or without them. A small disturbance can then precipitate formation of the jumps. At large bed wave amplitudes, the flow with jumps is the only one possible. The flow conditions and bed geometries over which the three different flows (jumps cannot form; jumps may or may not form; jumps will form) occur have not been delineated.

B. Distribution of Pressure Head on the Bed. Representative pressure-head distributions measured on Beds I and II are shown in figures 3A through 3D, and the amplitude ratios and phase shifts of the pressure waves are given in tables 2 and 3. The pressure is referred to that on the upstream crest of the wave on which measurements were made, and divided by the specific weight of water ($\gamma = \rho g$, where ρ is the fluid density and g the gravitational constant) to obtain the corresponding head. The amplitude ratios of the pressure waves are presented as the amplitude of the pressure-head variation divided by δ_o. For all flows except those which formed jumps the pressure wave is shifted almost exactly π relative to the bed wave.

An analytical expression for the pressure at any point in a wavy-bed flow has been derived by Iwasa and Kennedy (1968; their equation 20). Their relation expresses pressure as a function of the elevation of the point above the bed, bed slope and curvature, local depth and mean velocity of flow, depth gradient, and velocity distribution. It is the last dependence that make is difficult to predict the pressure distribution, for the nonuniform pressure gradients strongly affect the distribution of velocity, which in turn influences the pressure field. This problem and the difficulty it poses are discussed at length by Hsu and Kennedy (1971). Some analyses (not presented herein) of the pressure data presented in figures 3A through

3D and tables 2 and 3 revealed that a fairly reliable estimate of pressure can be obtained as the hydrostatic pressure plus the contribution due to curvature of a flow with a uniform velocity distribution; i.e., as

$$p_b = \rho g \eta + m\rho U^2 \eta \frac{d^2\delta}{dx^2} \qquad (10)$$

where m is a correction factor. For flows with bed and surface wave in phase (i.e., flows with large F), $m \simeq 1$. For low Froude number flows, with bed and surface waves out of phase, $m \simeq 1/2$.

C. Bed Shear Stress. Streamwise distributions of bed shear stress, measured along the center of the channel and normalized by $\rho U^2/2$, are presented in figures 1A through 1R for Runs 236 through 253, respectively. In tables 2 and 3 the amplitude, ζ_o, of the shear wave is half of the difference between the averages of the maxima and minima of the measured shear stresses, and the phase shift is the average of the upstream shifts between the bed crests and shear-stress maxima, and bed troughs and shear-stress minima. The mean shear stresses, $\bar{\tau}_o$, presented in tables 2 and 3, were calculated from the mean flow depth, flume width, and channel slope; these data are not particularly reliable because the short lengths of the wavy test sections and the nonuniform water surface profiles made it difficult to establish truly quasi-uniform flow, and to determine the energy gradient.

Prediction of the amplitudes and phase shifts of boundary shear stress for wavy boundary flows is a very complex problem, and has not yet been solved for even the somewhat simpler case of flow in wavy pipes. An extended review and discussion of the problem is presented by Hsu and Kennedy (1971). In figures 1A through 1R it is seen that the shear stress generally attains its maxima (minima) where the local depth is smallest (largest), and the velocity is greatest (least), as would be expected. However, close examination of the shear stress data shows that τ_o does not vary as the reciprocal of the depth squared, as might be expected for bed waves of small steepness. Consider, for example, figures 1K, 1M, and 1N, in which the depth is nearly constant but the shear stress is decidedly not constant. A further idea of the effects of boundary waviness on the shear stress can be obtained as follows. In Run 238, for example, the ratio of maximum to minimum shear stress is seen in figure 1C to be about two. The ratio of the square

of the maximum to the mean depth, on the other hand, is only about 1.2. The flow curvature and attendant pressure gradients and their effect on the velocity distribution are, of course, responsible for the amplification and distortion of the boundary shear stress undulation.

Finally it is perhaps noteworthy that the average shear stress, $\bar{\tau}_o$, is generally somewhat lower than the average of the shear stress measured streamwise along the channel centerline with the Preston tube. The bed centerline shear stress is much larger than that near the corners of the flow section, and hence is expected to be somewhat larger than $\bar{\tau}_o$. However, it should be borne in mind that, as noted above, the data on $\bar{\tau}_o$ are not regarded as particularly reliable.

D. Velocity and Total Head Distributions. Figures 4A through 4C and 4D through 4G present vertical distributions of mean velocity measured over Beds I and II, respectively, along the centerplane of the channel. The channel curvature is seen to have a seemingly disproportionate effect on the velocity distributions. The velocity profiles are generally much blunter over the bed-wave crests than over the troughs, as a consequence of the near-bed velocities being larger over the crests. This is a result of the pressure in the vicinity of the bed being increased over the troughs and decreased over the crests by the curvature of the flow. Hence near the bed the streamwise pressure gradient is negative from each bed-wave crest to the adjacent trough, then positive to the next crest, producing deceleration near the bed over the former reach and acceleration over the latter. As noted earlier the pressure at any point is dependent on the velocity distribution, which in turn is affected by the pressure field. Hence, rigorous formulation of the velocity distribution involves analysis of the equation of motion in the streamwise and normal directions. This has not yet been successfully accomplished even for the somewhat simpler case of flow in wavy-boundary closed conduits; the difficulties that arise are discussed at length by Hsu and Kennedy (1971). At and near the free surface, where the flow is locally nearly irrotational, the velocity increases with decreasing elevation; i.e., the Bernoulli sum is practically constant. This is no doubt the reason velocity is generally a maximum at the free surface at stations where the surface elevation is low, but has its maximum some distance below the free surface at stations of high surface elevation; an example of this situation is seen in figure 4A.

Downstream from the hydraulic jumps (see figure 4E) the velocity distributions are rather anomalous, and only begin to regain a more regular distribution just before the next downstream jump.

In their analysis of velocity distributions in close wavy-boundary flows, Hsu and Kennedy (1971) found that the streamwise momentum balance along a boundary wave is dominated by the variations in the momentum flux and pressure; i.e., the contribution to the momentum relation of the shear force and streamwise drag force exerted on the boundary wave is small compared to changes in momentum flux and the pressure forces. The boundary shear does, of course, largely balance the overall streamwise pressure gradient, and sets the "mean" velocity distribution about which the deviations occur. Likewise, in the case of free-surface wavy-bed flow the change in piezometric head between any two stations along a bed wave must be balanced predominantly by changes in the momentum flux since, except near the resonance point, the friction terms in (4) and (5) are relatively very small.

Logarithmic plots (not included herein) of velocity versus distance above the bed showedthat up to fairly large elevations above the bed -- generally to the point of maximum velocity -- the velocity distribution is well described by the power law,

$$\frac{u}{u_m} = \left\{\frac{y}{y(u_m)}\right\}^{1/n} \qquad (11)$$

where u is the velocity at elevation y above the bed, $y(u_m)$ is the elevation at which the maximum velocity u_m occurs, and 1/n is a nondimensional exponent. Note that n varies widely along each wavelength. Table 4 summarizes the values of n obtained from logarithmic plots of the velocity data presented in figures 4A through 4G.

Although no fully satisfactory analysis for predicting the velocity distribution has been developed, an estimate of the values of n can be made from the following calculation, which parallels that developed by Hsu and Kennedy (1971). As noted above, the surface velocity at any station can be calculated from the one-dimensional Bernoulli equation, using the Bernoulli sum at the water surface over, say, the adjacent upstream bed crest and the surface elevation at the station being examined. If it is assumed that the

power law can be extended to the water surface for determing the discharge, the unit discharge q, at any station is given by

$$q = Ud = u_s \int_0^{d+\eta} [y/(d+\eta)]^{1/n} \, dy \qquad (12)$$

where u_s is the surface velocity. Carrying out the integration in (12) yields, after some rearrangement,

$$n = \frac{Ud}{(\eta+d)u_s - Ud} \qquad (13)$$

Since in general $\eta << d$, (13) can be written

$$n = \frac{U}{u_s - U} \qquad (14)$$

Table 5 presents for two runs a comparison of measured values of n and those calculated from (14) with u_s for each station determined as described above. The agreement is as good as reasonably could be expected.

For steady, uniform flow, n in the power law is a function of only the local friction factor or the nondimensional boundary shear stress, $\tau_o/\rho\bar{u}^2$ where $\bar{u}$ is the mean velocity at the section, as is demonstrated by Hsu and Kennedy (1971). Hence it is of interest to inquire if the local value of n for nonuniform flows can be determined from the local boundary shear. Figure 5 shows for Run 239 (see table 4 and figure 4F) the measured values of n plotted against the local shear stress normalized by $\rho\bar{u}^2$. It is seen that there is pronounced hysteresis in the $n - \tau_o/\rho\bar{u}^2$ relation, which results from the local curvature and the convective effects on the velocity distribution Hsu and Kennedy (1971) obtained an empirical relation for the local friction factor for closed-conduit wavy boundary flow in terms of n, boundary slope, and boundary curvature for wavy-pipe flow.

Figures 6A and 6B show, respectively, the distribution of total head for Run 218 and an experiment with conditions close to those of Run 240. The head is measured relative to the total head at the free surface over the upstream crest, which in turn is referred to an arbitrary datum. The total head is seen to be very nearly constant along the free surface, as noted earlier. The effects of boundary curvature on the pressure distribution and hence also on the distributions of velocity and total head are clearly evident.

IV. CONCLUDING REMARKS

When the research program reported herein was initiated, in late 1966, it had as its goal determination and formulation of the phase shift, θ, between the bed and bed-shear-stress waves. This phase shift was then believed to be primarily responsible for the phase shift, and corresponding lag distance, between the local bed elevation and the local sediment transport rate. In Kennedy's (1963, 1969) theory for the formation of sedimentary bed forms, a lag between the local transport rate and local bed elevation is essential to the occurrence of interfacial instability. One can make a supportable argument (or so it then seemed) that the local sediment transport rate and local bed shear stress should have similar distributions along a wavy bed, at least for bed waves of very small steepness. If this were proven to be the case, elucidation of the shift between the bed and shear-stress waves would clarify the lag between the bed and sediment-transport-rate waves. Resolution of the latter question would, in turn, eliminate one of the principal stumbling blocks to development of a predictor for the occurrence of the different types of bed forms.

Shortly after this investigation was begun, the complementary study of turbulent flow in wavy-walled circular conduits which has been reported by Hsu and Kennedy (1971) was commenced. It was found that the internal structure of wavy-boundary flows could be studied much more advantageously in the closed-conduit air flow than in the open channel flow of water. Turbulence measurements could readily be made in air, the axisymmetric pipe flow was free of the secondary currents produced in wavy-bed open channel flow (Robillard and Kennedy, 1967), and the internal composition of the flow was not complicated by the presence of the stationary free-surface waves. On the other hand, the water-surface configuration could not, of course, be studied in the conduit flow.

Thus as the two research programs developed, attention was focused on the internal structure of the wavy pipe flow and on the free-surface configuration of the open-channel flow. The data from the former study (Hsu and Kennedy, 1971) showed, among other things, that the maxima in the intensities of the components of the turbulence velocities do not occur at the same wave-phase positions as the greatest boundary shear stress. The

shear stress maxima occurs just upstream from the wave crests (sections of smallest diameter), while the longitudinal component of the turbulence is a maximum near the wave troughs and the other two components peak at other phase positions. Hence it appears that the maxima of the individual turbulence components are reached at different positions than the maximum of the cross-correlation between the axial and radial components, which determines the shear stress. Since the local turbulent entrainment rate must be strongly related to the radial turbulence component, the distributions of boundary shear stress and sediment transport rate cannot be expected to be similar. The relation between boundary geometry and turbulent heat transfer has been treated at length by Ashton (1971). In his study of the formation of ice ripples by turbulent flows he found that the heat-transfer-rate undulation is shifted relative to the interfacial wave by a constant fraction (approximately 3/4) of the wavelength plus a variable distance that appears to be a linear inverse function of the inverse of the flow velocity. Whether a comparable relationship holds for the distribution of sediment transport rate remains to be seen.

The several investigations of wavy-boundary end related flows conducted to date have demonstrated that boundary curvature and streamwise pressure gradients have a great effect on the rates of turbulent transfer of heat, matter, momentum, etc. but the individual contributions of boundary curvature and slope, and their interaction, are not yet well understood. Progress has been made toward a better understanding of the effects of just flow convergence or divergence on the turbulence structure of diffuser flows (Schlichting, 1968). Boundary curvature appears to have a much more complex effect on the turbulence, and is not nearly so well understood. The formation of Göertler vortices is a complicating factor that surely has a large effect on turbulent transfer near concave boundaries. It appears that before further progress can be made toward understanding the effects of boundary curvature on the turbulence structure of flows, some cleverly conceived and adroitly executed experiments will have to be conducted. In particular, it might be of value to undertake some heat transfer experiments in turbulent, annular Couette flow, driven by a cylindrical shell near the center of the annular channel. This experimental setup would offer constant curvature without the complication of nonuniformity. Moreover, data could be obtained for both concave and convex boundaries.

The present investigation has clearly demonstrated that Iwasa and Kennedy's (1968) third-order approximation to the linearized one-dimensional energy equation gives an adequate description of the free-surface configuration of open-channel wavy-bed flows, except near the resonant Froude number or velocity. However, for conditions close to resonance, the flow is complicated by the formation of a hydraulic jump over each bed wave (Robillard and Kennedy, 1967), and no formulation which does not allow for the occurrence of these jumps will not be valid for near-resonant flows. Hence, there would appear to be little reason, other than academic interest, for pursuing higher-order analyses of conditions near resonance for nondissipative flows; a realistic mathematical model of near-resonant conditions must include the energy loss through and momentum balance across the jumps. It would be of interest, however, to have the conditions for the initiation of jumps accurately delineated, as this would in turn provide a criterion for the breaking of stationary waves which occur above antidunes.

REFERENCES

Ashton, G.D., 1971. *The formation of ice ripples on the underside of river ice covers,* Ph.D. Dissertation, Dept. of Mechanics and Hydraulics, The Univ. of Iowa, Iowa City, Iowa.

Benjamin, T.B., 1959. "Shearing flow over a wavy boundary," *J. Fluid Mech.*, 6, 161-205.

Engelund, F., and Hansen, E., 1966. "Investigation of flow in alluvial streams," *Hydraulic Laboratory, Technical University of Denmark,* Bulletin 9, Copenhagen.

Gupta, A.K., and Mollo-Christensen, E.L., 1966. "An experimental investigation of air flow over a wavy plate," *Mass. Inst. of Tech.,* Research report, Cambridge, Mass.

Hansen, E., 1969. Discussion of "Free surface shear flow over a wavy bed," by Iwasa Y., and Kennedy, J.F., *Proc. ASCE, Jour. of Hyd. Div.*, 95, HY1, 526-530.

Hsu, S.T. and Kennedy, J.F., 1971. "Turbulent flow in wavy pipes," *J. Fluid Mech.*, 47, 481-502.

Iwasa, Y., and Kennedy, J.F., 1968. "Free surface shear flow over a wavy bed," *Proc. ASCE, Jour. of Hyd. Div.*, 94, HY2, 431-454.

Iwasa, Y., and Kennedy, J.F., 1970. Closure discussion of "Free surface shear flow over a wavy bed," by Iwasa,Y. and Kennedy, J.F., *Proc. ASCE, Jour. of Hyd. Div.*, 96, HY3, 837-841.

Kennedy, J.F., 1963. "The mechanics of dunes and antidunes in erodible-bed channels," *J. Fluid Mech.*, 16, 521-544.

Kennedy, J.F., 1969. "The formation of sediment ripples, dunes, and antidunes," *Ann. Rev. of Fluid Mech.*, 1, 147-168.

Lamb, H., 1932. *Hydrodynamics,* 6th ed., Cambridge University Press, Cambridge.

Mei, C., 1969. "Steady free surface flow over wavy bed," *Proc. ASCE, Jour. Hyd. Div.*, 95, EM6, 1393-1402.

Milne-Thomson, L.M., 1960. *Theoretical Hydrodynamics,* 4th ed., The MacMillan Co., New York.

Motzfeld, H., 1937. "Die turbulente strömung an Welligen Wänden," *ZAMM,* 17, 193-212.

Nielsen, H.B., 1970. "A second order approximation to free surface shear flow over a wavy bed," *Hydraulic Laboratory and Numeric Institute, Technical University of Denmark,* Lyngby.

Rechenberg, I., Schwefel, H.P. and Bienert, P., 1967. "Messung kleiner wandschubspannunger bei turbulenten Grenzschichten in Ablosenähe," *Hermann Föttinger Institute für Strömungstenchnik, T.U. Berlin,* Berlin.

Rhyming, I.L., 1963. "Non-equilibrium flow inside a wavy cylinder," *J. Fluid. Mech.*, 17, 551-560.

Robillard, L., 1965. *Free surface shear flow over a wavy bed,* S.M. Thesis, Dept. of Civil Eng., Mass. Inst. of Tech., Cambridge, Mass.

Robillard, L., and Kennedy, J.F., 1967. "Some experimental observations on free surface shear flow over a wavy boundary," *Proc. 12th Congress of Int. Assn. for Hyd. Res.*, Ft. Collins, Colo.

Schlicting, H., 1968. *Boundary Layer Theory,* 6th ed., McGraw-Hill, New York.

Sigal, A., 1971. *An experimental investigation of the turbulent boundary layer over a wavy wall,* Ph.D. Dissertation, Guggenheim Lab, Cal. Inst. of Tech., Pasadena, Cal.

Stanton, T., Marshall, D., and Houghton, R., 1932. "The growth of waves on water due to the action of wind," *Proc. Roy. Soc.*, A137, 283-293.

Vincenti, W.G., 1959. "Non equilibrium flow over a wavy wall," *J. Fluid Mech.*, 6, 481-496.

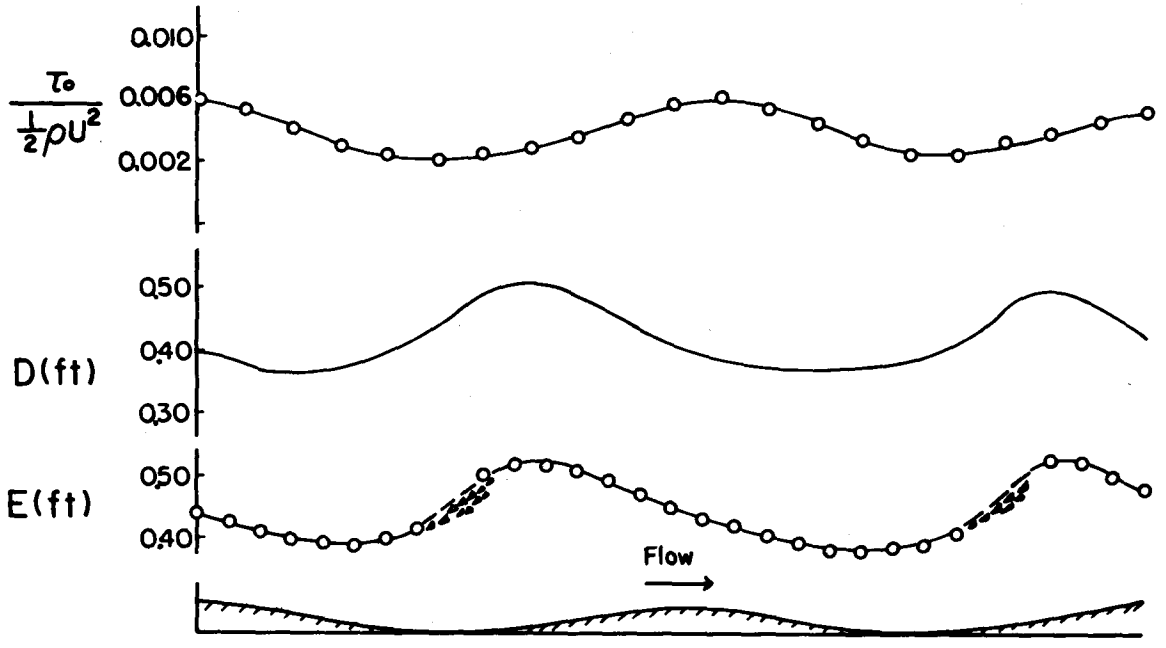

Figure 1A Streamwise distributions of water surface elevation, depth, and normalized boundary shear flow for Run 236. d = 0.420 ft, U = 2.92 fps, F = 0.81, $\bar{\tau}$ = 0.016 psf

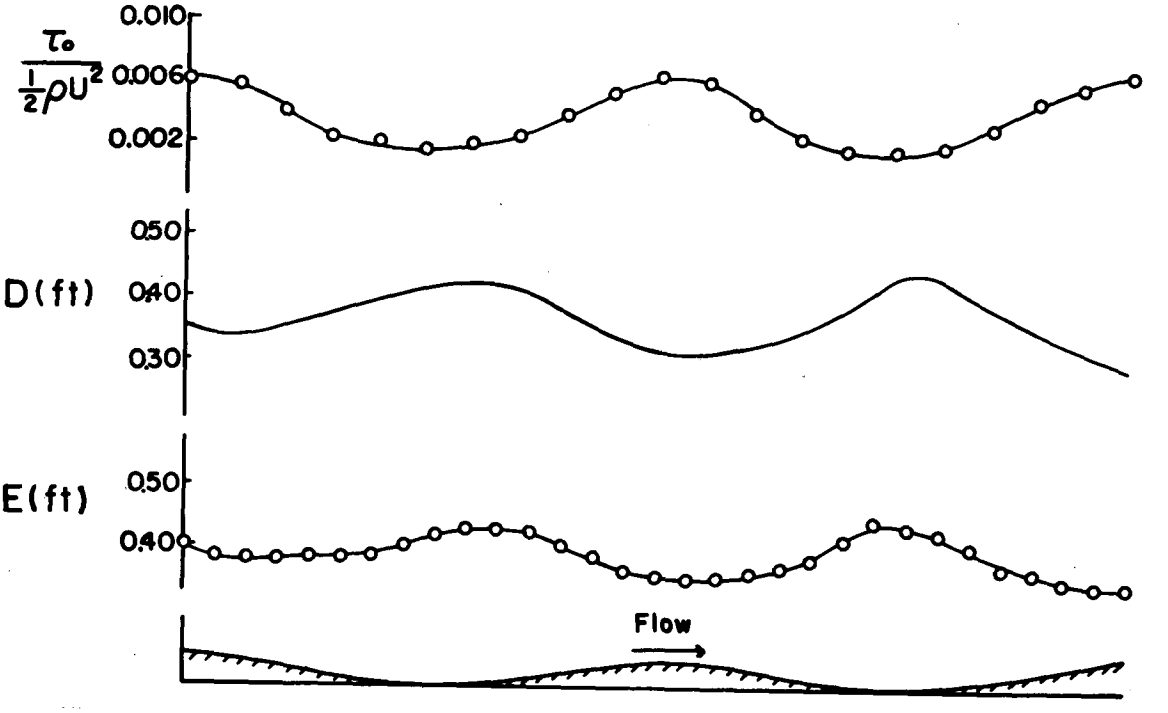

Figure 1B Streamwise distributions of water surface elevation, depth, and normalized boundary shear flow for Run 237. d = 0.375 ft, U = 2.70 fps, F = 0.86, $\bar{\tau}$ = 0.014 psf

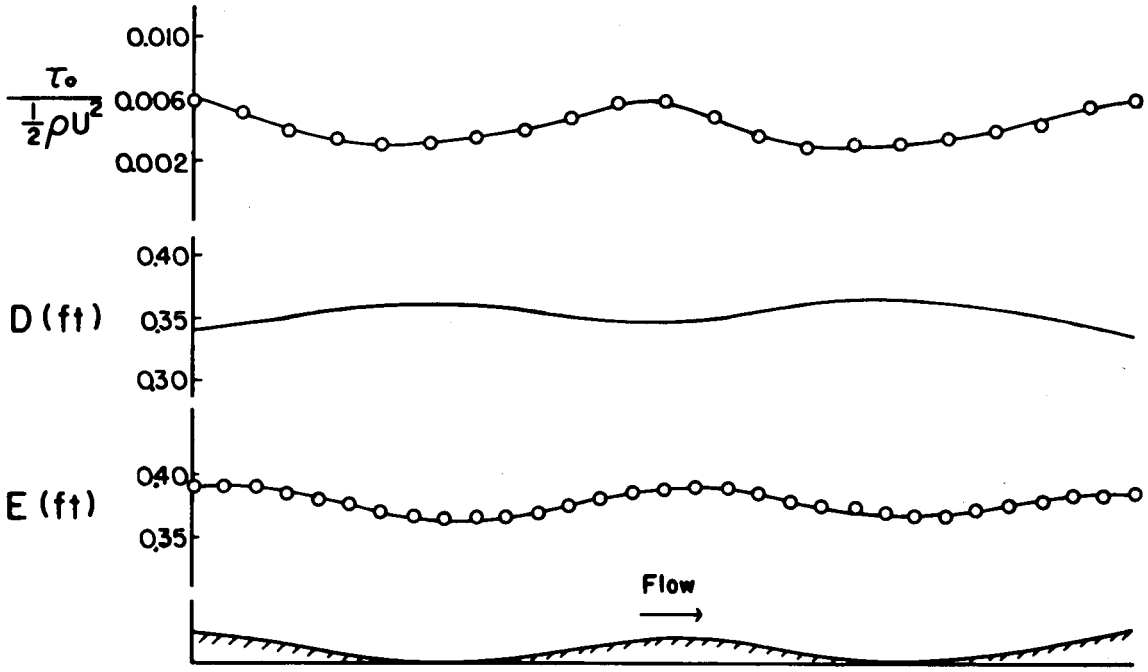

Figure 1C Streamwise distributions of water surface elevation, depth, and normalized boundary shear flow for Run 238. d = 0.340 ft, U = 4.65 fps, F = 1.42, $\bar{\tau}$ = 0.039 psf

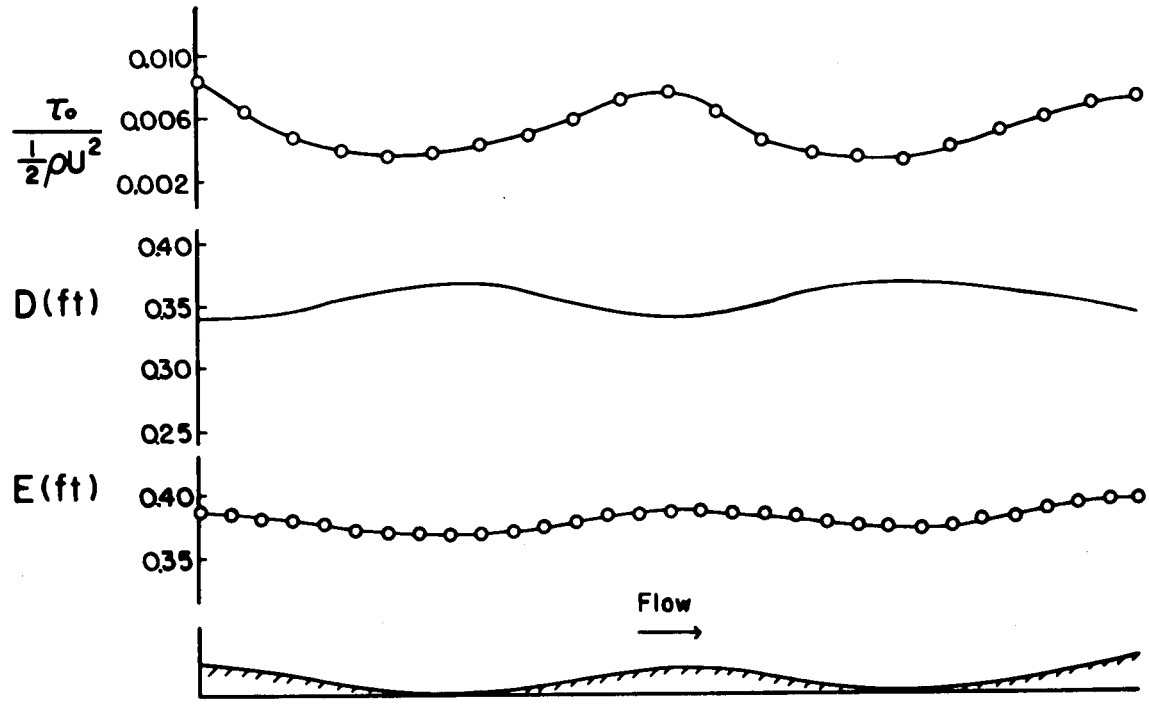

Figure 1D Streamwise distributions of water surface elevation, depth, and normalized boundary shear flow for Run 239. d = 0.355 ft, U = 4.68 fps, F = 1.42, $\bar{\tau}$ = 0.053 psf

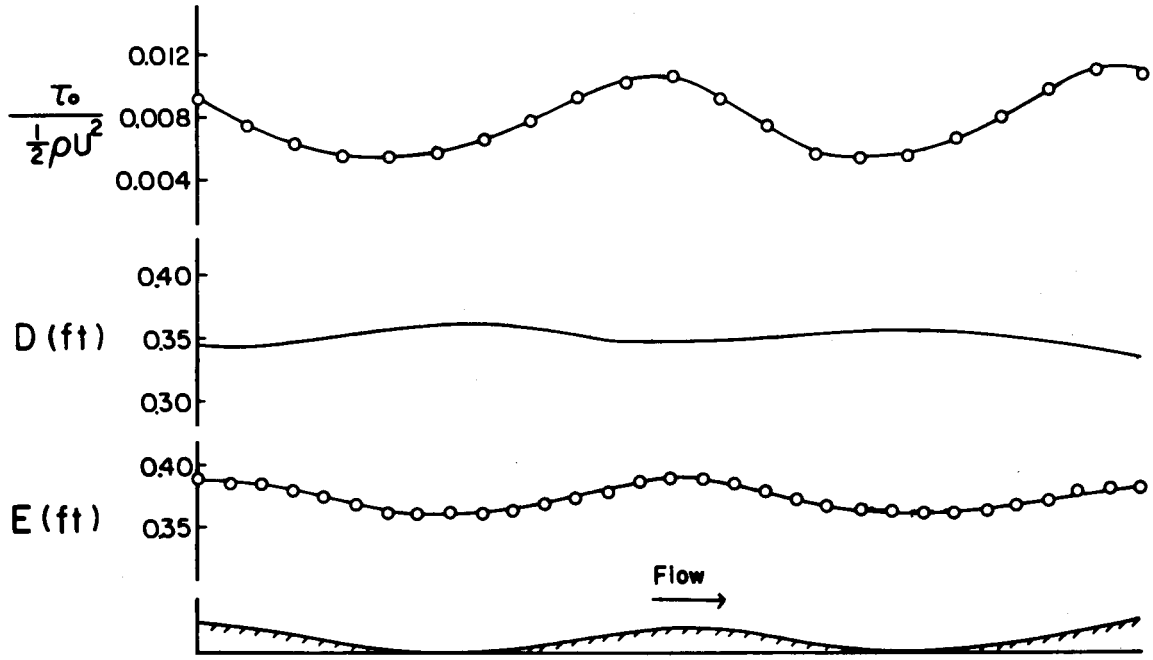

Figure 1E Streamwise distributions of water surface elevation, depth, and normalized boundary shear flow for Run 240. d = 0.345 ft, U = 4.24 fps, F = 1.29, $\bar{\tau}$ = 0.035 psf

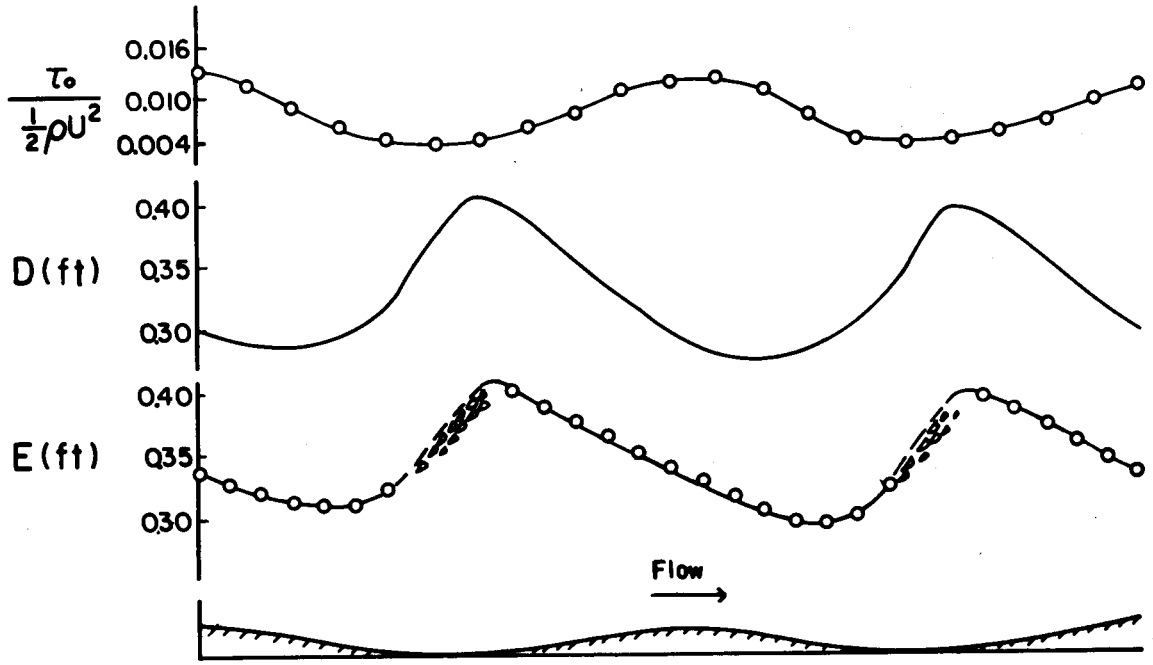

Figure 1F Streamwise distributions of water surface elevation, depth, and normalized boundary shear flow for Run 241. d = 0.345 ft, U = 2.00 fps, F = 0.61, $\bar{\tau}$ = 0.016 psf

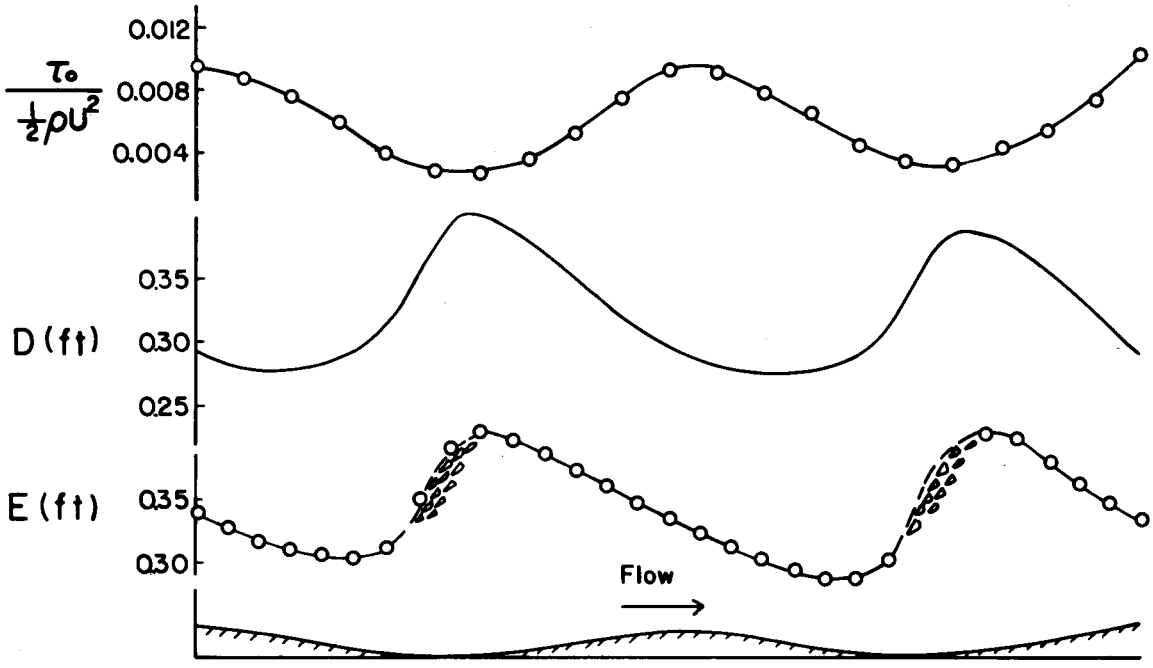

Figure 1G Streamwise distributions of water surface elevation, depth, and normalized boundary shear flow for Run 242. d = 0.340 ft, U = 2.51 fps, F = 0.77, $\bar{\tau}$ = 0.035 psf

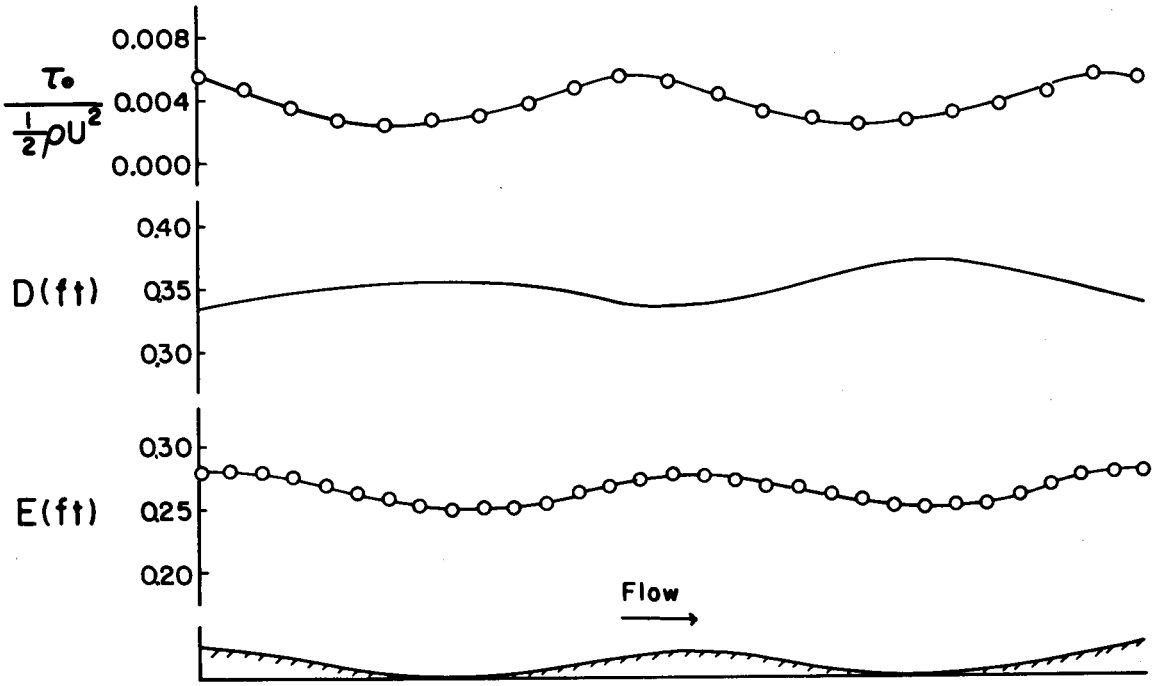

Figure 1H Streamwise distributions of water surface elevation, depth, and normalized boundary shear flow for Run 243. d = 0.345 ft, U = 5.21 fps, F = 1.59, $\bar{\tau}$ = 0.098 psf

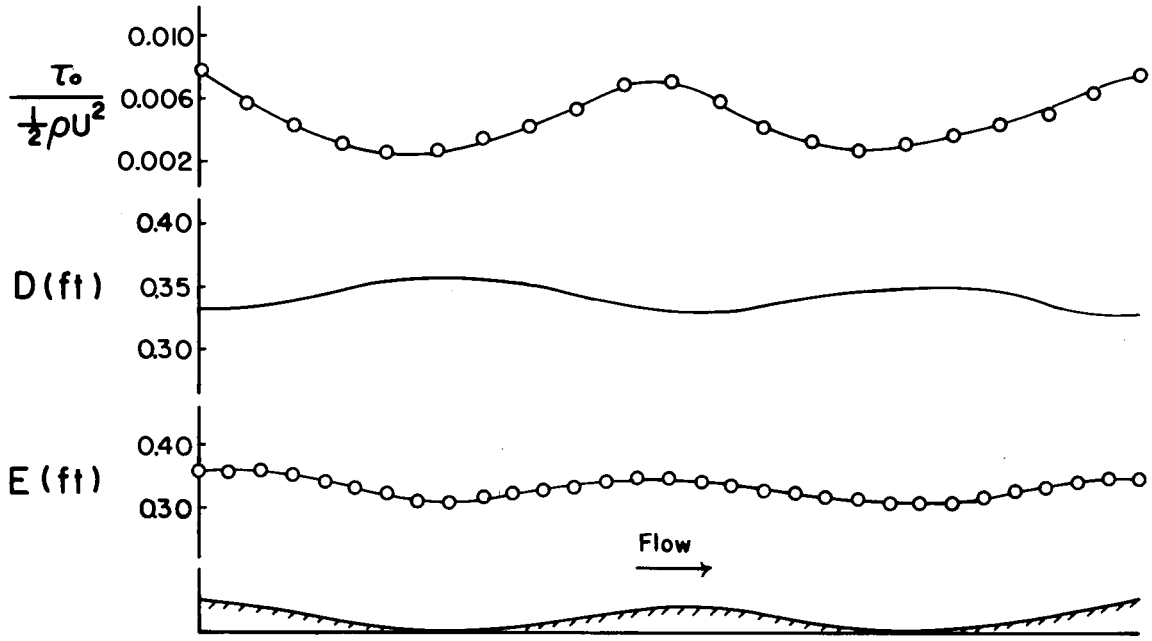

Figure 1I Streamwise distributions of water surface elevation, depth, and normalized boundary shear flow for Run 244. d = 0.345 ft, U = 5.37 fps, F = 1.61, $\bar{\tau}$ = 0.125 psf

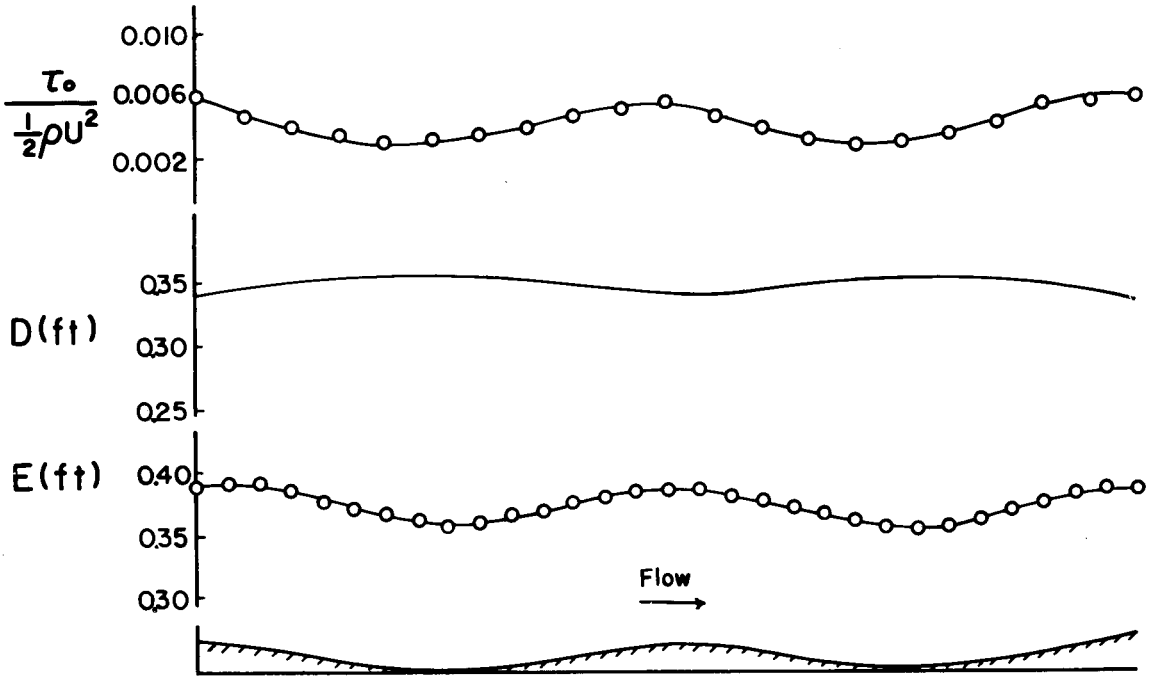

Figure 1J Streamwise distributions of water surface elevation, depth, and normalized boundary shear flow for Run 245. d = 0.340 ft, U = 3.79 fps, F = 1.16, $\bar{\tau}$ = 0.060 psf

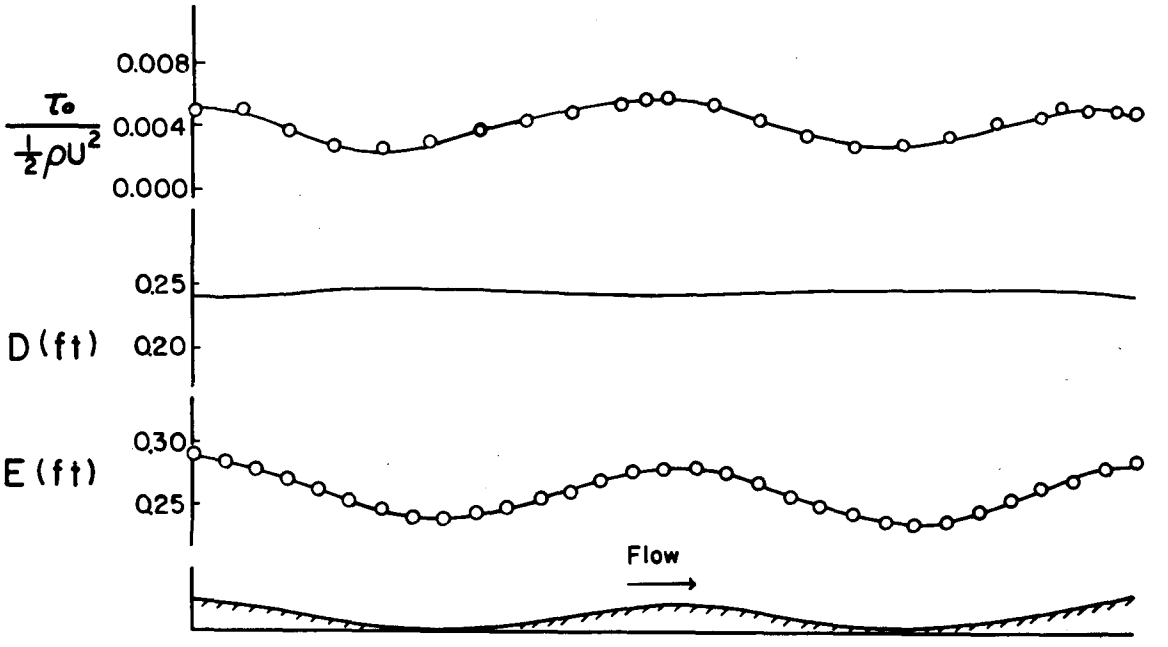

Figure 1K Streamwise distributions of water surface elevation, depth, and normalized boundary shear flow for Run 246. d = 0.347 ft, U = 4.40 fps, F = 1.48, $\bar{\tau}$ = 0.070 psf

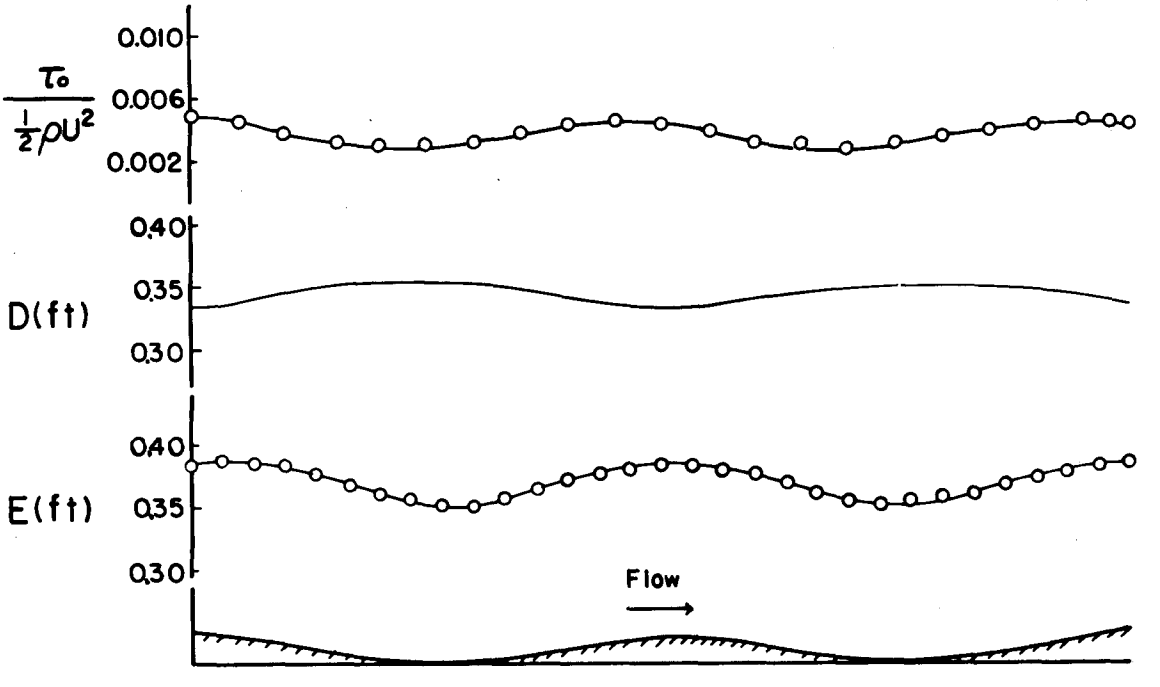

Figure 1L Streamwise distributions of water surface elevation, depth, and normalized boundary shear flow for Run 247. d = 0.330 ft, U = 3.83 fps, F = 1.18, $\bar{\tau}$ = 0.051 psf

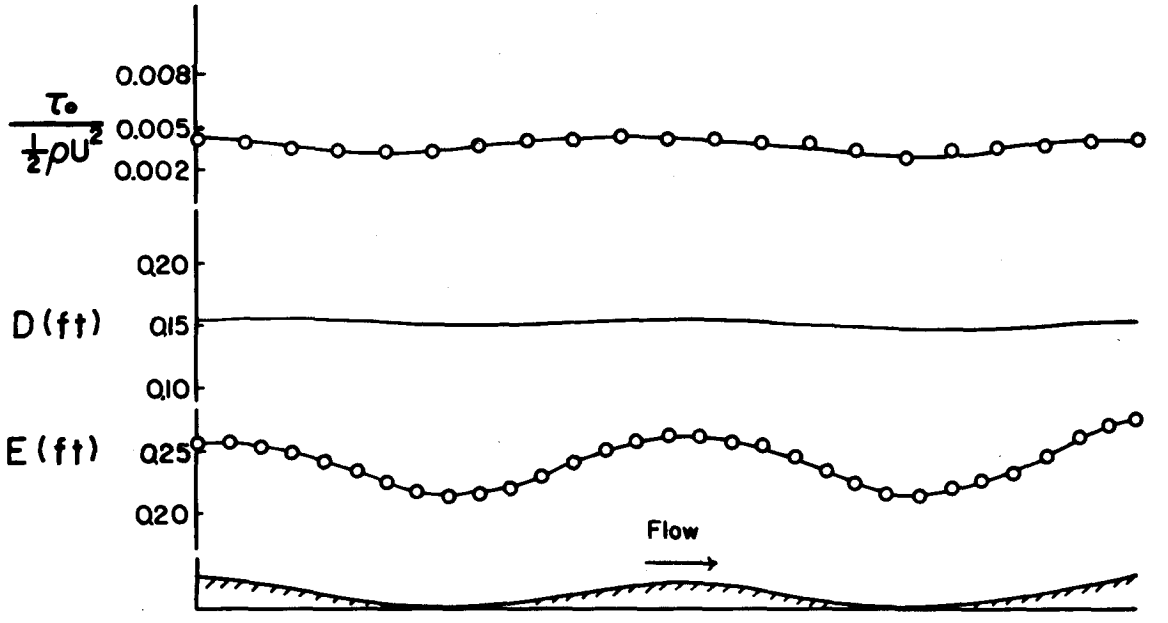

Figure 1M Streamwise distributions of water surface elevation, depth, and normalized boundary shear flow for Run 248. d = 0.210 ft, U = 2.64 fps, F = 1.40, $\bar{\tau}$ = 0.044 psf

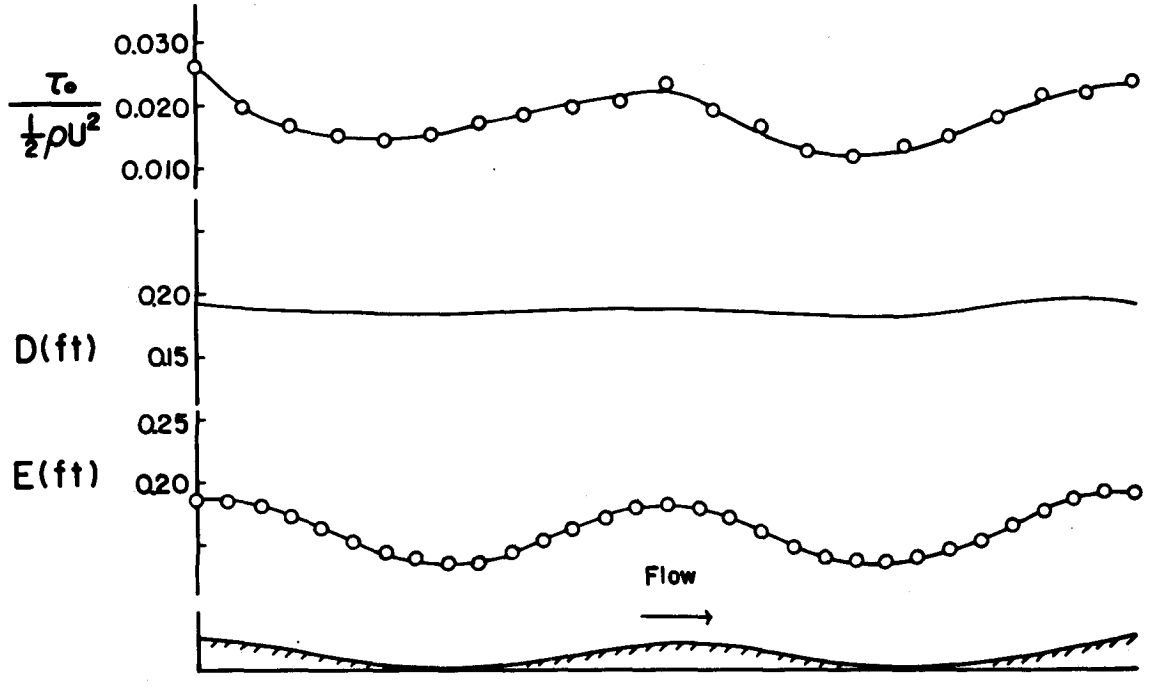

Figure 1N Streamwise distributions of water surface elevation, depth, and normalized boundary shear flow for Run 249. d = 0.190 ft, U = 3.64 fps, F = 1.47, $\bar{\tau}$ = 0.056 psf

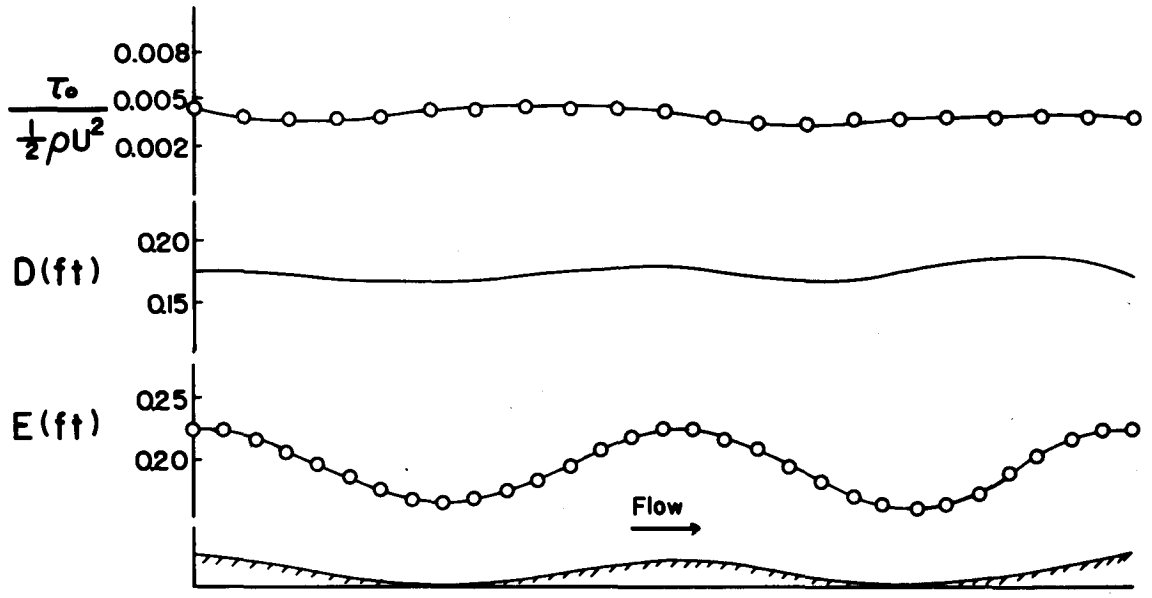

Figure 10 Streamwise distributions of water surface elevation, depth, and normalized boundary shear flow for Run 250. d = 0.165 ft, U = 3.66 fps, F = 1.58, $\bar{\tau}$ = 0.048 psf

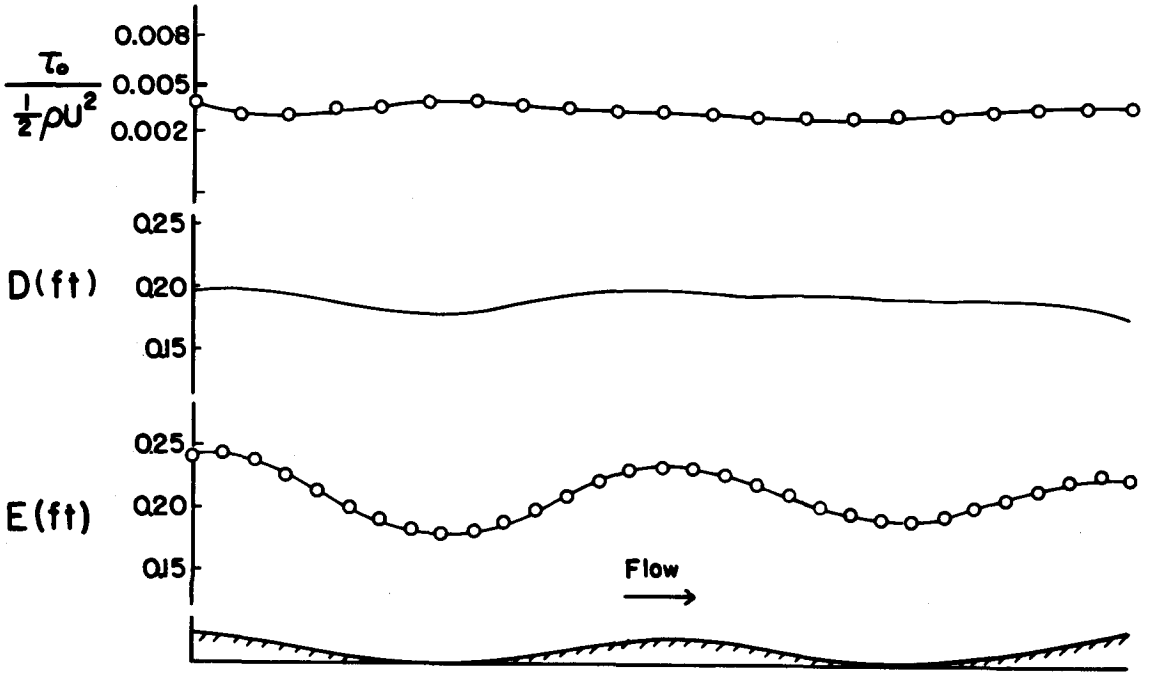

Figure 1P Streamwise distributions of water surface elevation, depth, and normalized boundary shear flow for Run 251. d = 0.180 ft, U = 3.19 fps, F = 1.33, $\bar{\tau}$ = 0.034 psf

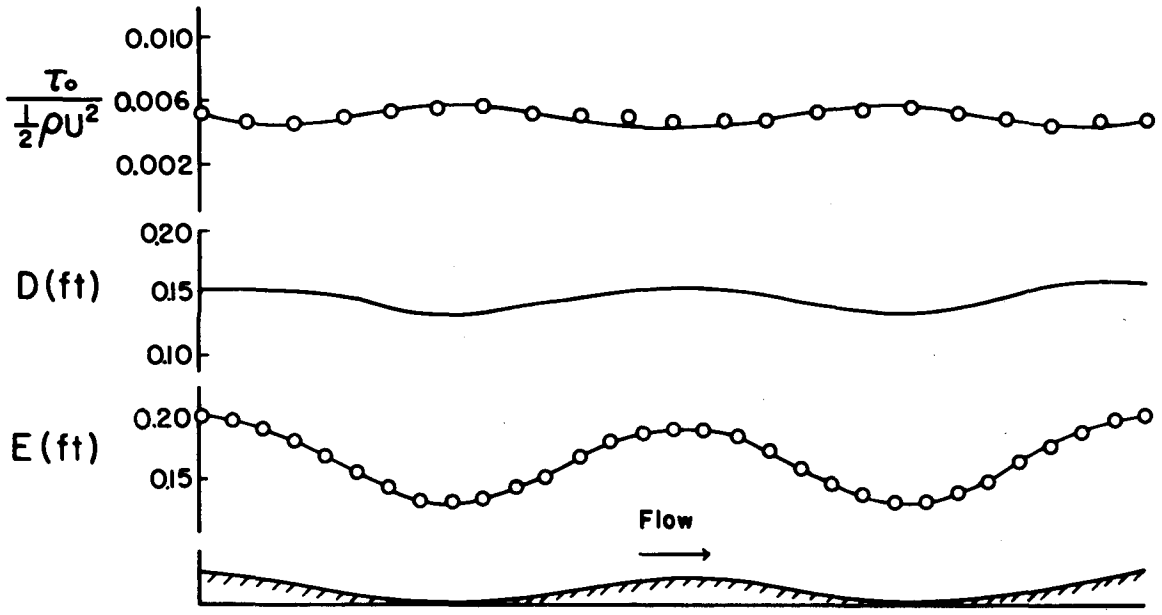

Figure 1Q Streamwise distributions of water surface elevation, depth, and normalized boundary shear flow for Run 252. d = 0.140 ft, U = 3.11 fps, F = 1.47, $\bar{\tau}$ = 0.048 psf

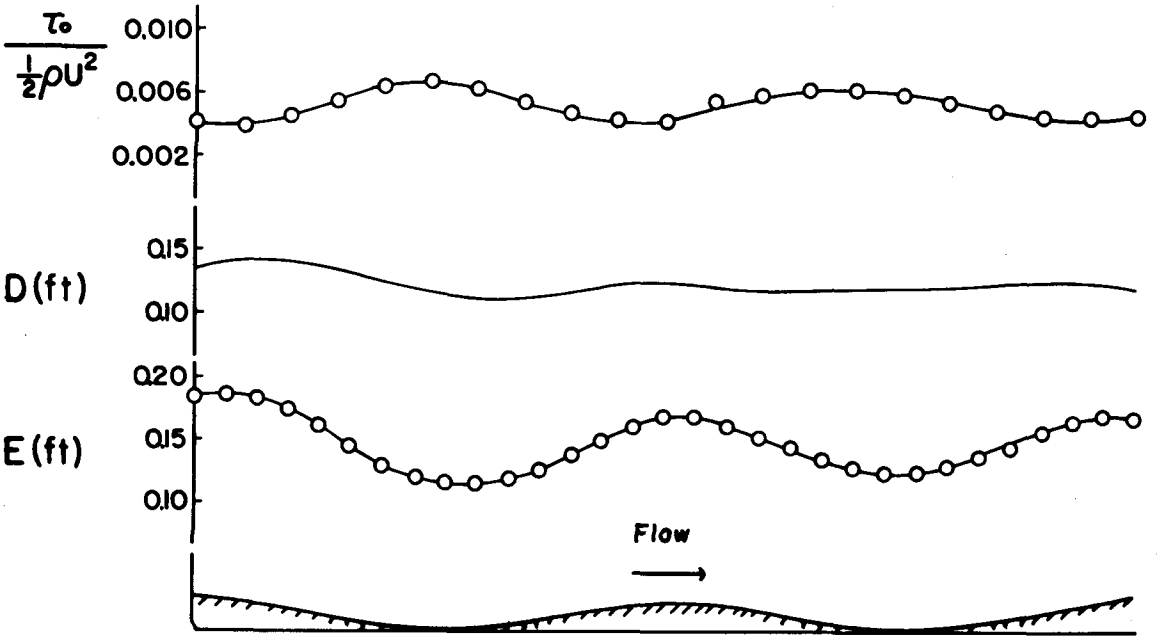

Figure 1R Streamwise distributions of water surface elevation, depth, and normalized boundary shear flow for Run 253. d = 0.120 ft, U = 2.63 fps, F = 1.35, $\bar{\tau}$ = 0.035 psf

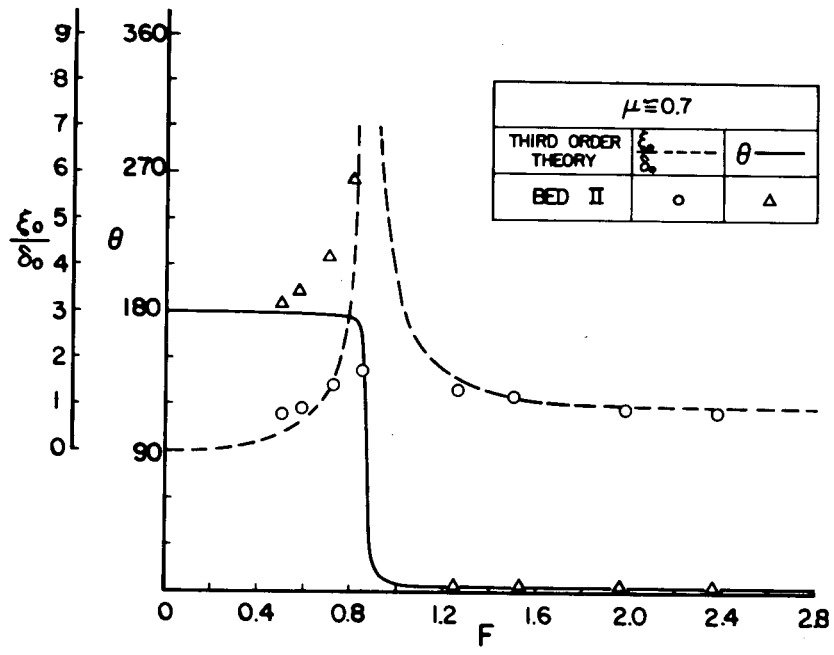

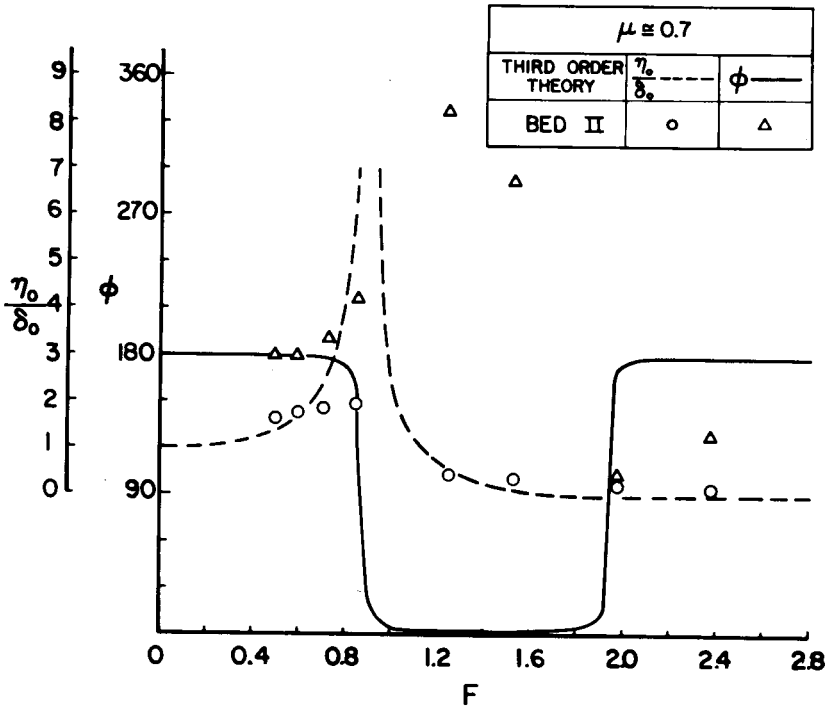

Figure 2A Comparison of predicted and measured amplitude ratios and phase shift of surface and depth waves. $\mu \cong 0.7$

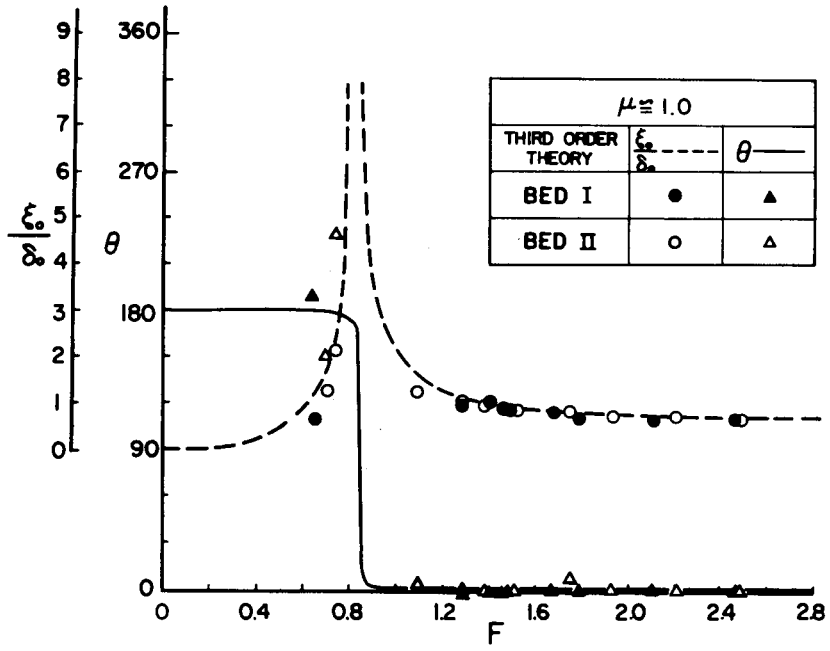

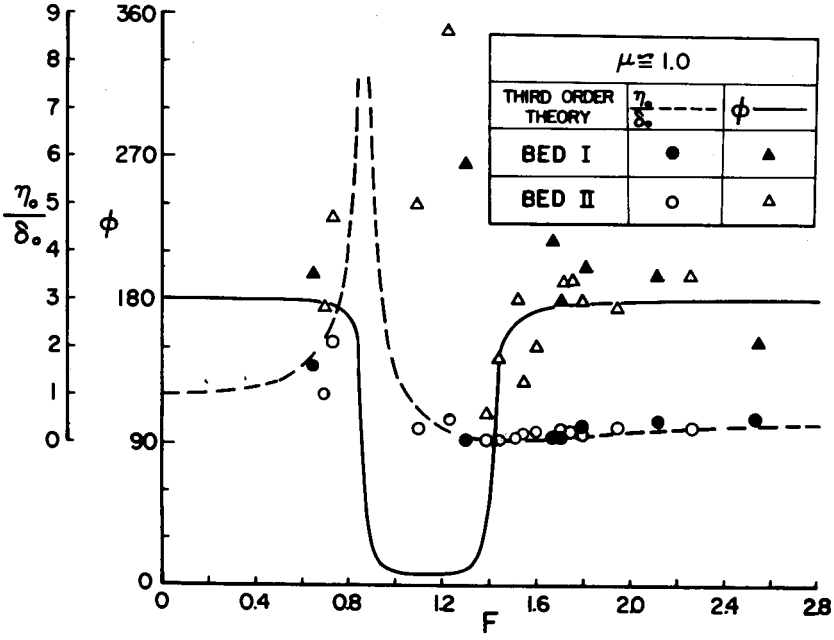

Figure 2B Comparison of predicted and measured amplitude ratios and phase shift of surface and depth waves. $\mu \cong 1.0$

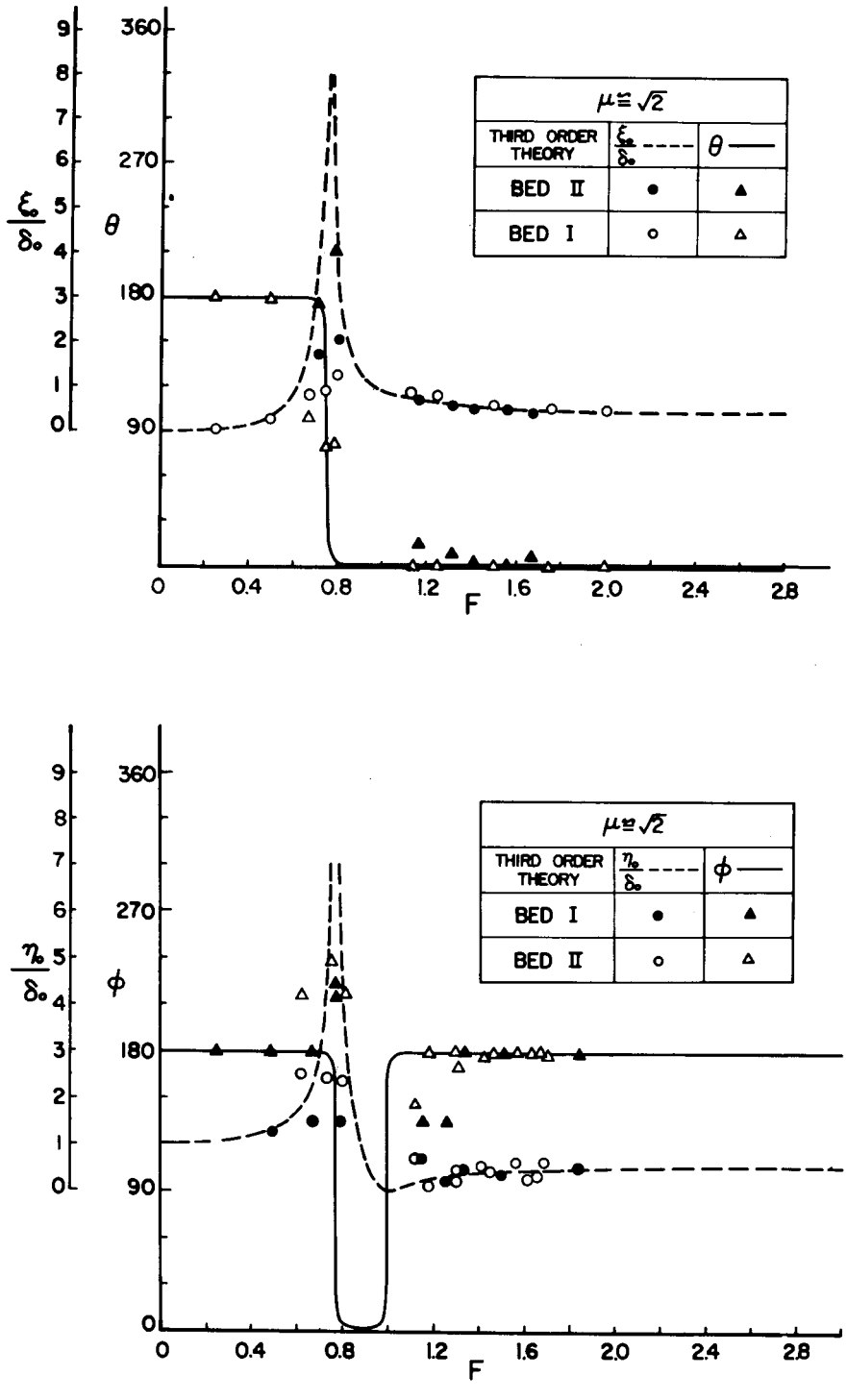

Figure 2C Comparison of predicted and measured amplitude ratios and phase shift of surface and depth waves. $\mu \cong \sqrt{2}$

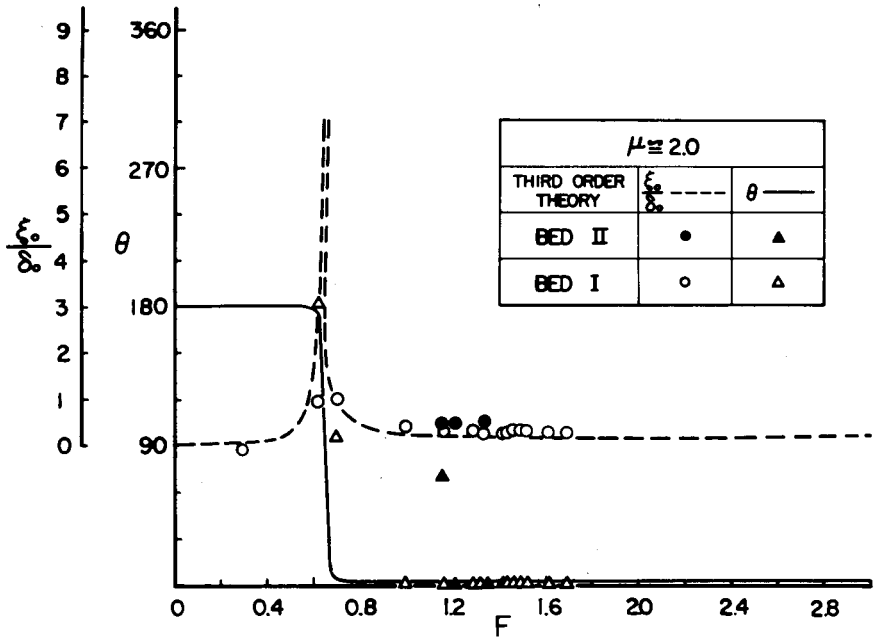

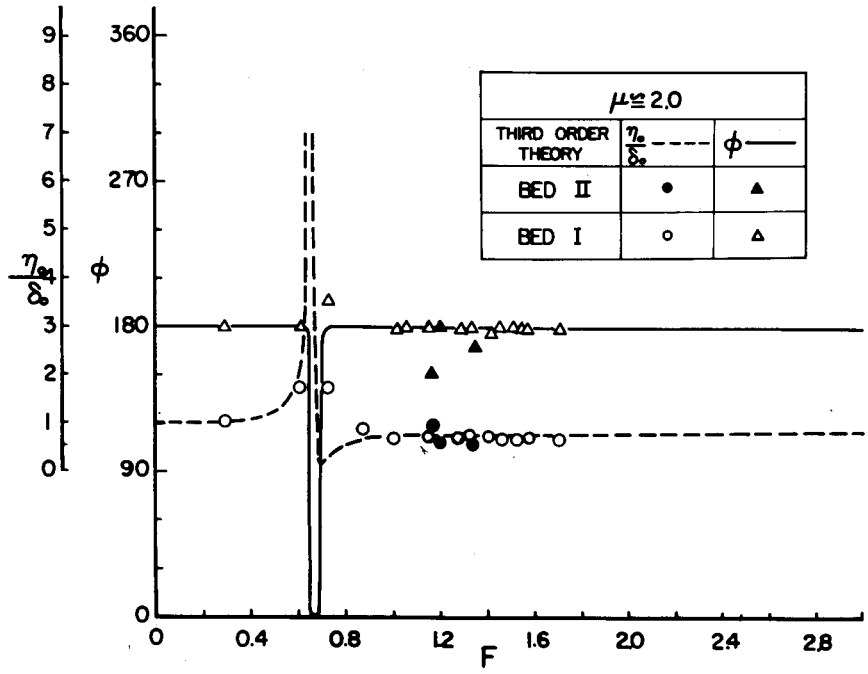

Figure 2D Comparison of predicted and measured amplitude ratios and phase shift of surface and depth waves. $\mu \cong 2.0$

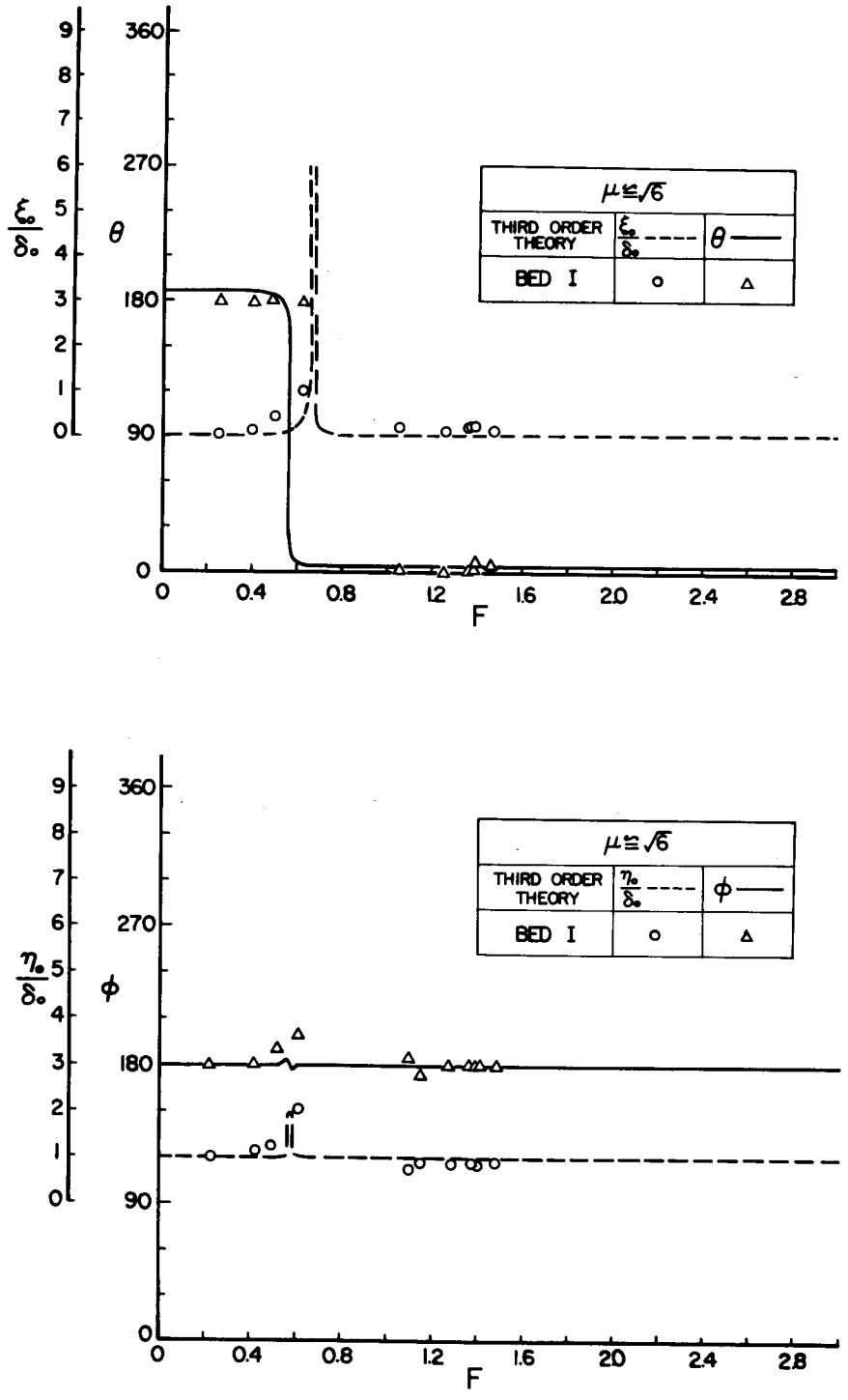

Figure 2E Comparison of predicted and measured amplitude ratios and phase shift of surface and depth waves. $\mu \cong \sqrt{6}$

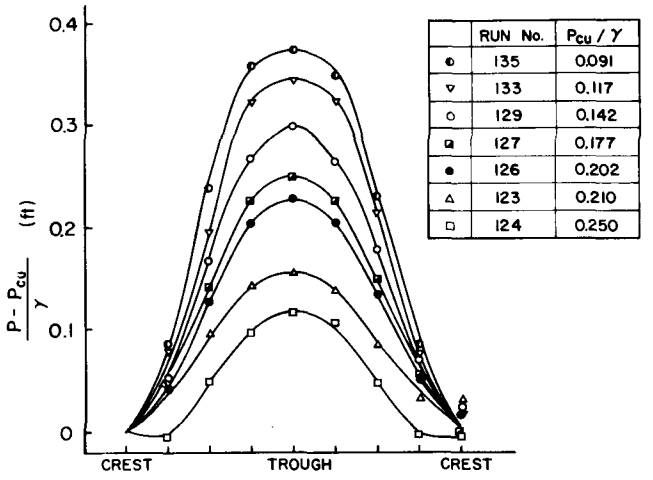

Figure 3A Distribution of pressure-head. Bed I. $\mu \cong 2.0$

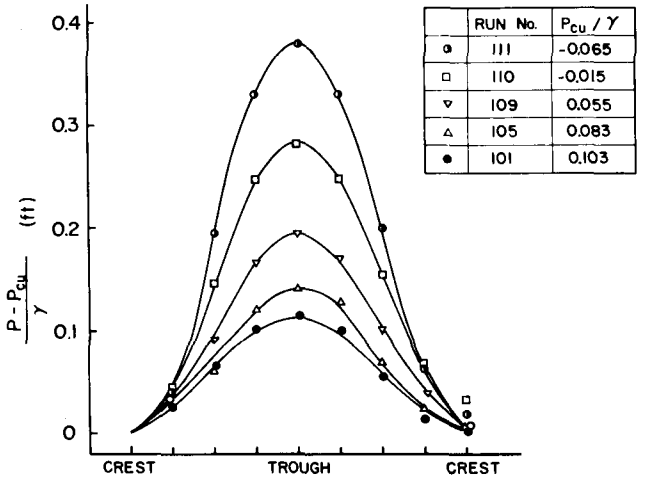

Figure 3B Distribution of pressure-head. Bed I. $\mu \cong 1.0$

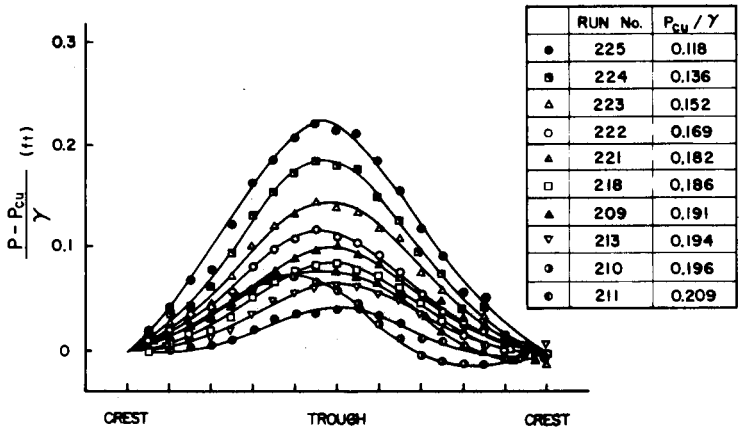

Figure 3C Distribution of pressure-head. Bed II. $\mu \cong 1.0$

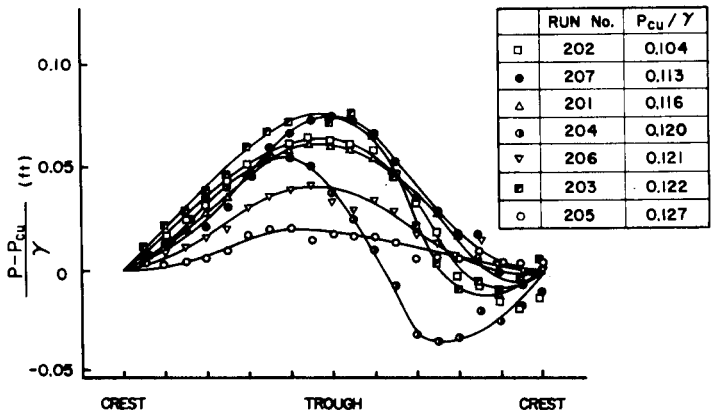

Figure 3D Distribution of pressure-head. Bed II. $\mu = 0.667$

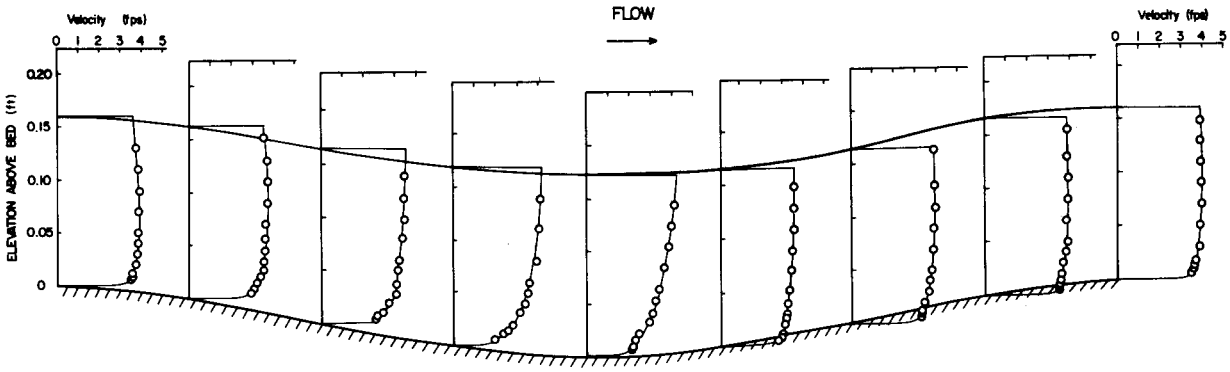

Figure 4A Velocity distribution for flow over Bed I. Run No. 106, $\mu = 1.06$, $F = 1.46$

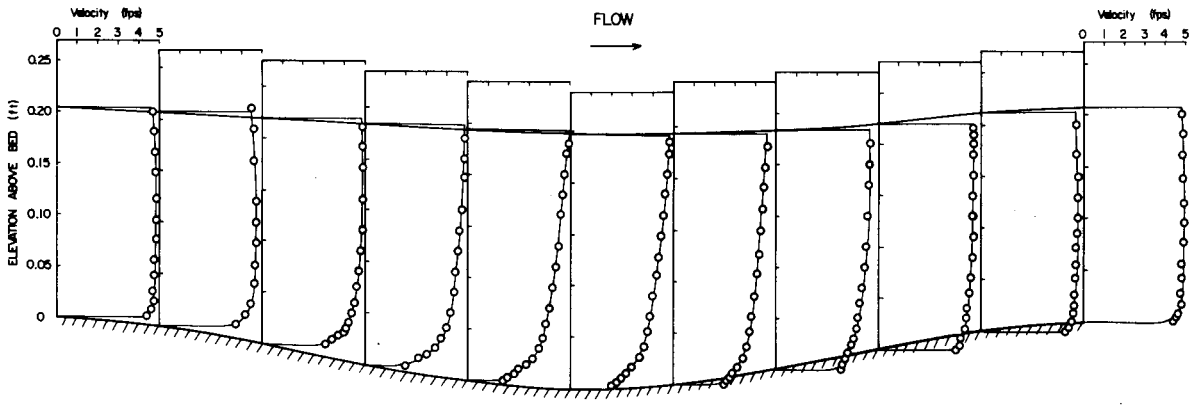

Figure 4B Velocity distribution for flow over Bed I. Run No. 115, $\mu = 1.49$, $F = 1.31$

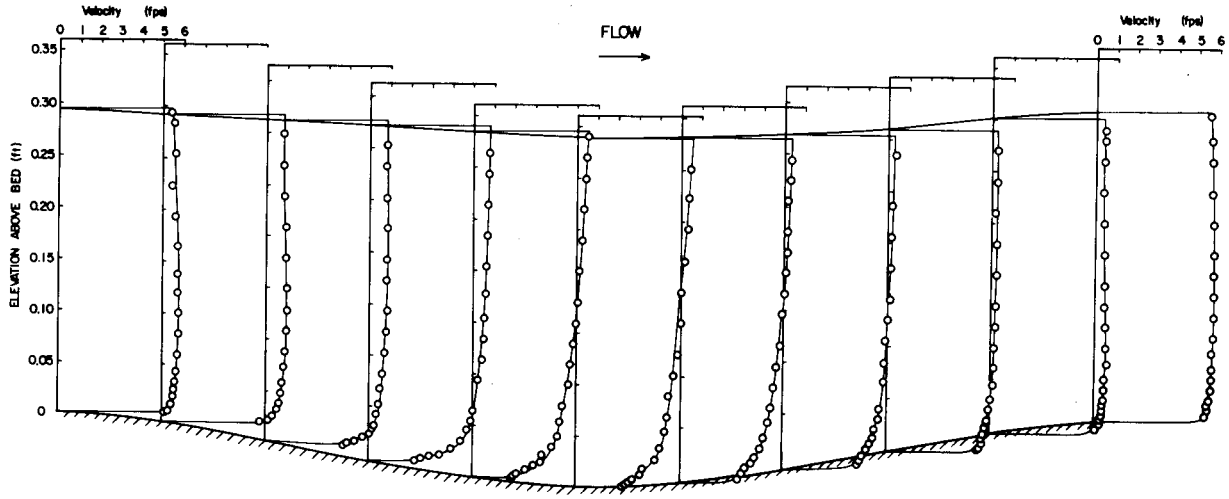

Figure 4C Velocity distribution for flow over Bed I. Run No. 132. $\mu = 2.01$, $F = 1.49$

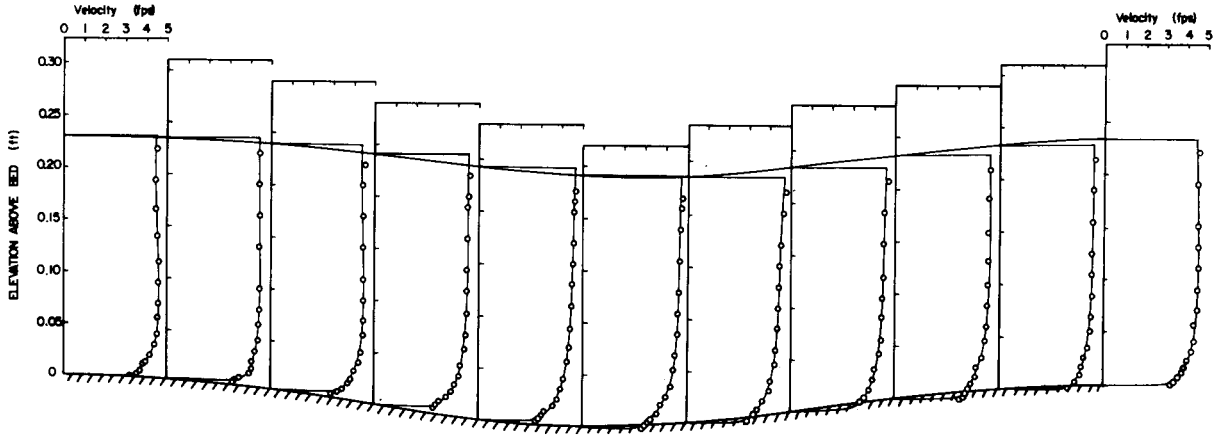

Figure 4D Velocity distribution for flow over Bed II. Run No. 217, $\mu = 1.0$, $F = 1.5$

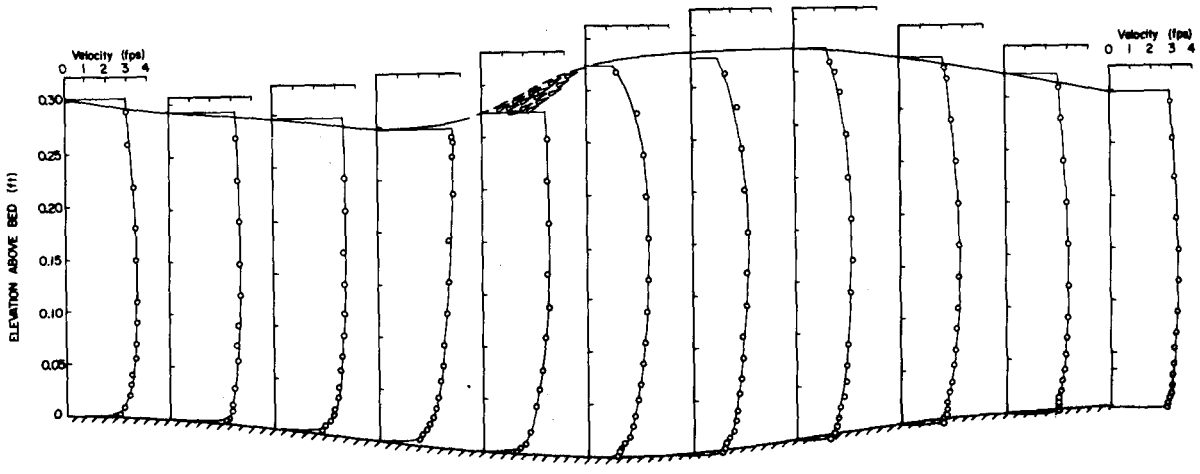

Figure 4E Velocity distribution for flow over Bed II. Run No. 227, $\mu = 1.39$, $F = 0.79$

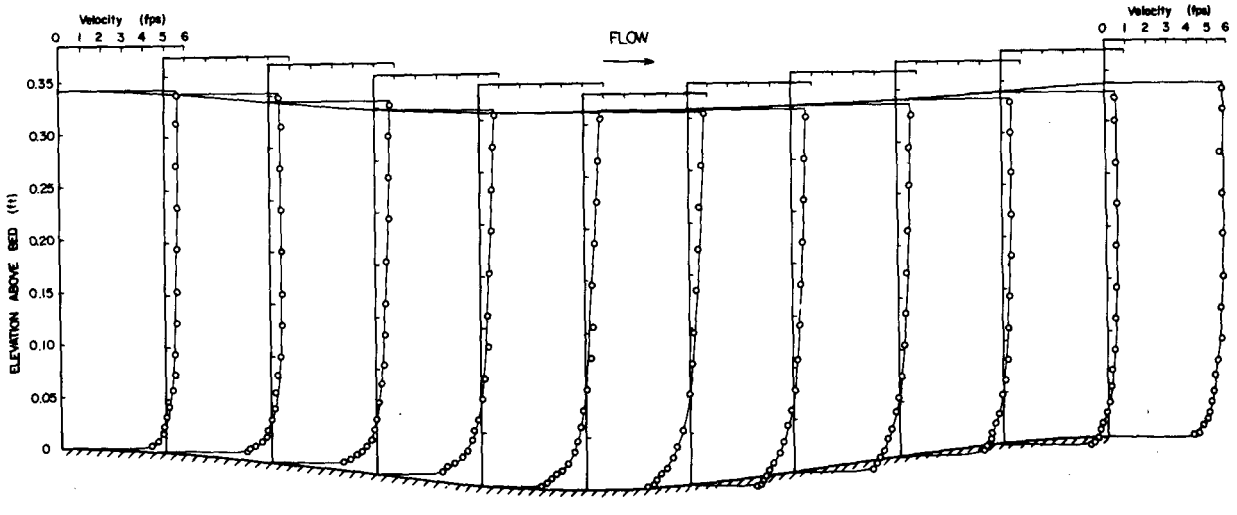

Figure 4F Velocity distribution for flow over Bed II. Run No. 239, $\mu = 1.5$, $F = 1.5$

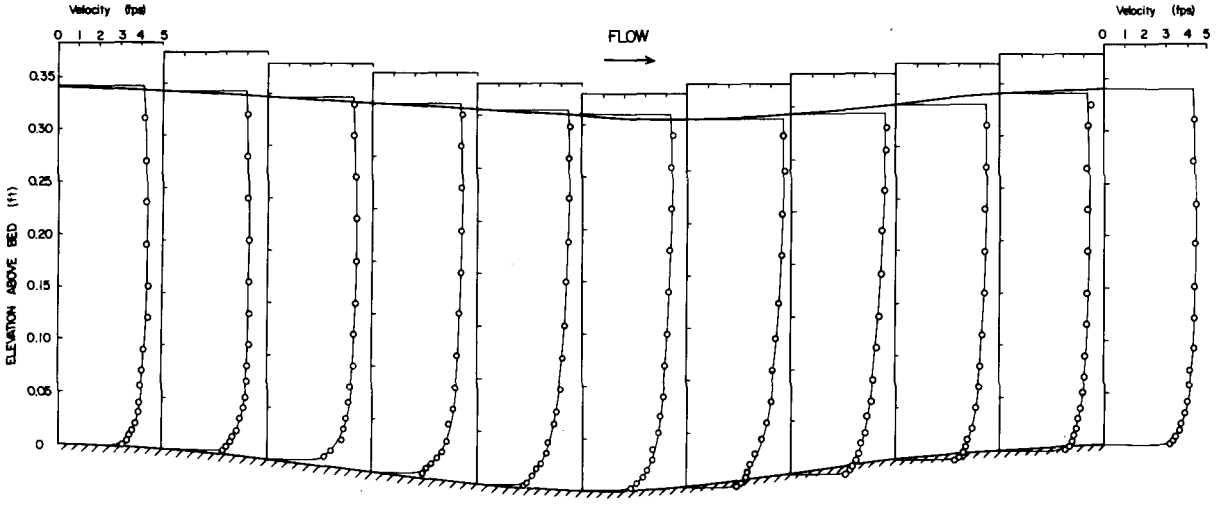

Figure 4G Velocity distribution for flow over Bed II. Run No. 240, $\mu = 1.5$, $F = 1.1$

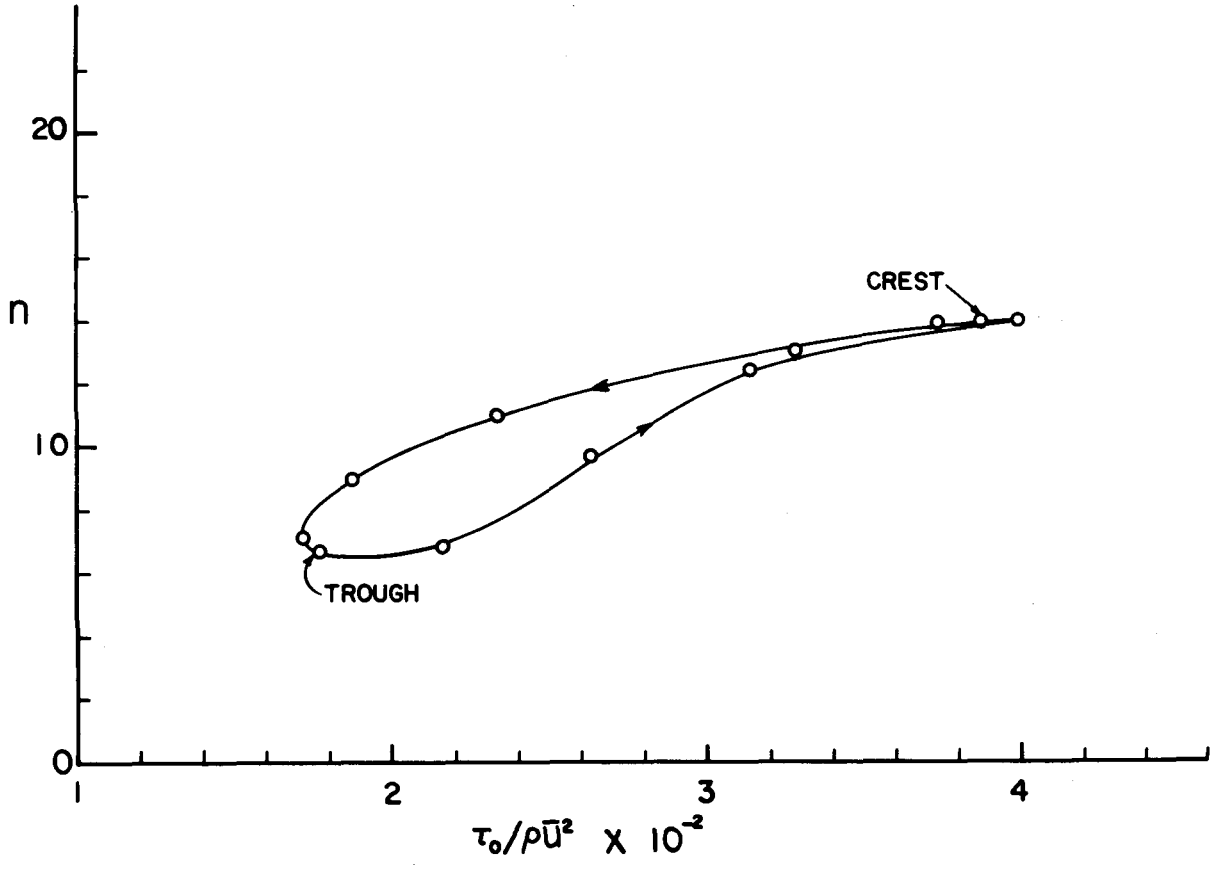

Figure 5 Relation between n and $\tau_o/\rho\bar{u}^2$ for Run 249

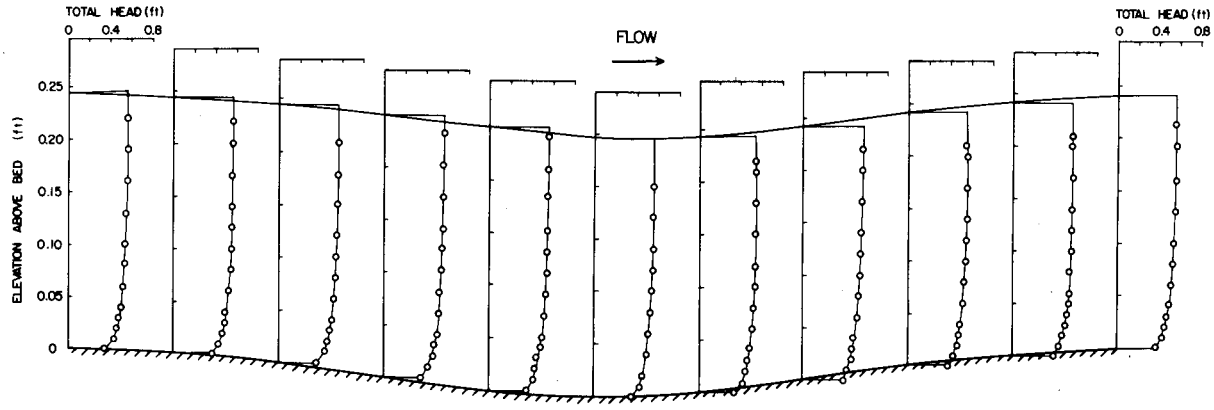

Figure 6A Distribution of total head for Run 218

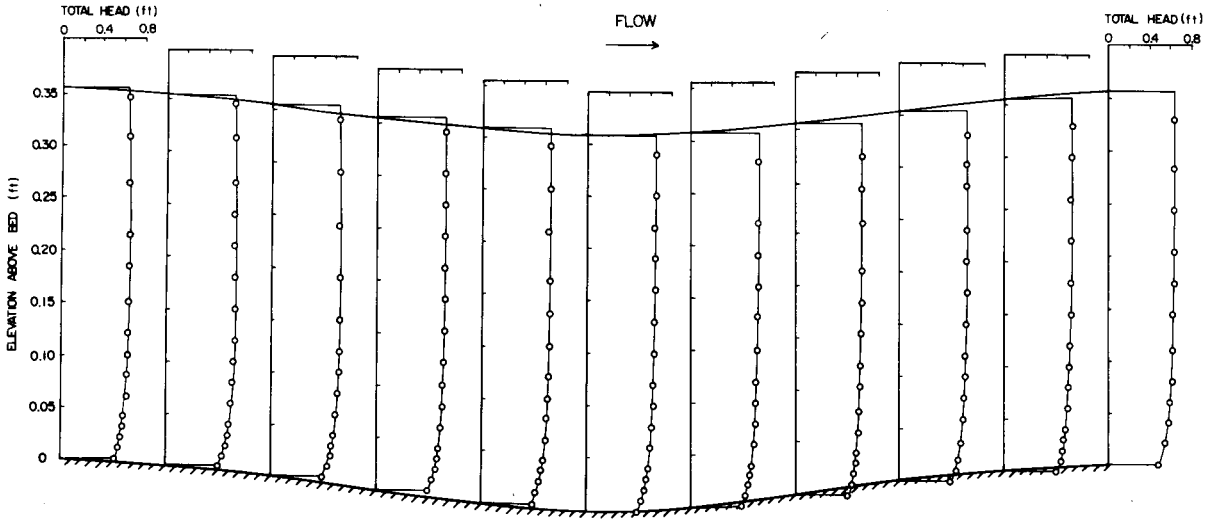

Figure 6B Distribution of total head for flow with properties close to those of Run 240, Bed II, $\mu = 1.5$, $F = 1.1$, $d = 0.36$ ft

Table 3. Summary of Results Obtained in Experiments with Bed II

Run No.	Nondimensional Wave Number	Froude Number	Mean Velocity	Mean Water Depth	Mean Shear Stress	Depth Wave		Surface Wave		Bed Pressure-Head Wave		Shear Wave		Remarks
						Amplitude Ratio	Phase Shift	Amplitude Ratio	Phase Shift	Amplitude Ratio	Phase Shift	Amplitude	Phase	
	μ	F	U	d	$\bar{\tau}_o$	η_o/δ_o	ϕ	ζ_o/δ_o	θ	σ_o/δ_o	β	ζ_o	α	
			ft/sec	ft	lb/ft^2		Degrees		Degrees		Degrees	lb/ft^2	Degrees	
201	0.65	0.50	1.13	0.155	--	1.68	174	0.86	180	1.2	180	--	--	3 surface waves over each bed wave
202	0.66	0.59	1.33	0.158	--	1.75	180	0.92	195	1.5	180	--	--	Jumps
203	0.69	0.71	1.61	0.165	--	1.88	192	1.34	213	1.8	180	--	--	Irregular waves with jumps
204	0.68	0.85	1.93	0.162	--	1.98	216	1.80	261	2.0	126	--	--	Jumps
205	0.67	1.25	2.82	0.159	--	0.41	336	1.36	0	0.4	180	--	--	
206	0.67	1.53	3.47	0.159	--	0.46	292	1.21	0	0.72	162	--	--	
207	0.67	1.98	4.48	0.161	--	0.14	104	0.91	0	1.44	180	--	--	
208	0.66	2.38	5.38	0.158	--	0.18	144	0.83	0	--	--	--	--	
209	1.00	0.70	1.95	0.240	--	0.96	172	1.28	150	1.7	162	--	--	Jumps
210	1.00	0.73	2.02	0.240	--	2.15	230	2.15	230	1.4	126	--	--	
211	1.00	1.09	3.05	0.242	--	0.23	240	1.22	3	1.0	180	--	--	
212	1.00	1.19	3.31	0.240	--	0.5	348	0.82	0	--	--	--	--	
213	1.00	1.29	3.58	0.240	--	0.2	266	1.0	0	1.4	180	--	--	Depth wave not readily measured
214	1.00	1.31	3.64	0.238	--	--	--	0.9	0	--	--	--	--	
215	1.00	1.38	3.81	0.239	--	0.1	108	0.92	0	--	--	--	--	
216	1.00	1.40	3.89	0.240	--	0.15	144	0.86	24	--	--	--	--	
217	1.00	1.50	4.27	0.238	--	0.20	125	0.7	20	--	--	--	--	
218	1.00	1.52	4.38	0.240	--	0.24	180	0.88	0	1.86	180	--	--	
219	1.00	1.60	4.61	0.240	--	0.28	160	0.66	24	--	--	--	--	
220	1.00	1.70	4.69	0.238	--	0.30	192	0.64	12	--	--	--	--	
221	1.01	1.75	4.88	0.242	--	0.28	192	0.80	9	2.0	180	--	--	
222	1.00	1.79	4.96	0.239	--	0.33	180	0.68	0	2.44	162	--	--	
223	1.00	1.93	5.38	0.240	--	0.33	174	0.70	0	3.00	162	--	--	
224	1.00	2.22	6.17	0.240	--	0.34	195	0.70	0	3.83	162	--	--	
225	1.00	2.48	6.89	0.241	--	0.50	195	0.64	0	5.65	162	--	--	
226	1.38	0.73	2.38	0.330	--	2.42	180	1.78	177	--	--	--	--	
227	1.39	0.79	2.58	0.332	--	2.46	216	2.08	213	--	--	--	--	Weak jumps
228	1.42	1.16	3.85	0.339	--	0.68	144	0.70	15	--	--	--	--	
229	1.42	1.30	4.31	0.339	--	0.41	168	0.60	9	--	--	--	--	
230	1.42	1.41	4.67	0.339	--	0.47	174	0.53	3	--	--	--	--	
231	1.41	1.56	5.12	0.337	--	0.51	180	0.51	0	--	--	--	--	
232	1.42	1.68	5.55	0.339	--	0.54	177	0.46	9	--	--	--	--	
233	1.96	1.15	4.47	0.470	--	1.00	150	0.50	72	--	--	--	--	
234	1.95	1.33	5.16	0.465	--	0.50	168	0.50	0	--	--	--	--	
235	2.00	1.21	4.76	0.480	--	0.52	180	0.40	0	--	--	--	--	
236	1.76	0.81	2.92	0.420	0.016	4.52	256	2.80	256	--	--	0.034	36	Jumps
237	1.57	0.86	2.70	0.375	0.013	2.64	--	1.50	--	--	--	0.034	0	Surface unsteady
238	1.42	1.42	4.65	0.340	0.039	0.4	180	0.52	0	--	--	0.064	0	
239	1.49	1.42	4.68	0.355	0.053	0.50	180	0.42	0	--	--	0.080	0	
240	1.44	1.29	4.24	0.345	0.035	0.30	180	0.62	0	--	--	0.052	0	
241	1.44	0.61	2.0	0.345	0.016	2.40	216	2.5	0	--	--	0.017	216	Jumps
242	1.42	0.77	2.51	0.340	0.035	2.70	240	2.04	240	--	--	0.019	0	Jumps
243	1.44	1.59	5.21	0.345	0.098	0.40	180	0.62	0	--	--	0.016	336	
244	1.44	1.61	5.37	0.345	0.125	0.48	180	0.48	0	--	--	0.065	0	
245	1.42	1.16	3.79	0.340	0.060	0.22	180	0.58	0	--	--	0.021	0	
246	1.03	1.48	4.40	0.347	0.070	0.12	180	0.90	0	--	--	0.019	336	
247	1.38	1.18	3.83	0.330	0.051	0.30	180	0.60	0	--	--	0.015	324	
248	0.88	1.40	3.64	0.210	0.044	0.10	--	0.90	0	--	--	0.008	0	
249	0.80	1.47	3.64	0.190	0.056	0.13	--	0.50	0	--	--	0.010	0	
250	0.69	1.58	3.66	0.165	0.048	0.30	12	1.10	0	--	--	0.005	240	
251	0.75	1.33	3.19	0.180	0.034	0.42	0	1.2	0	--	--	0.006	336	
252	0.59	1.47	3.11	0.140	0.048	0.40	0	1.24	0	--	--	0.006	180	
253	0.50	1.35	2.63	0.120	0.035	0.20	--	1.1	336	--	--	0.007	180	

Table 4. Summary of Exponents, n, in Power Law Distributions of Velocity Profiles Shown in Figures 4A - 4G.

Run No.	106	115	132	217	227	239	240
Froude No.	1.46	1.31	1.49	1.50	0.79	1.42	1.44
Wave No.	1.06	1.49	2.01	1.00	1.39	1.49	1.29
Fig. No.	4A	4B	4C	4D	4E	4F	4G
Station							
Crest	16.8	34.2	66.8	11.0	14.6	14.0	13.8
0.10 L		24.9	25.4	11.0	16.1	13.0	10.7
0.125L	14.2						
0.20 L		11.6	16.1	10.2	10.2	11.2	8.2
0.25 L	5.3						
0.30 L		6.5	8.3	8.4	7.5	9.0	7.3
0.375L	3.8						
0.40 L		4.7	4.6	8.0	6.3	7.1	6.3
0.50 L	3.4	3.7	4.1	9.0	5.5	6.8	6.7
0.60 L		7.1	7.2	9.3	6.3	6.8	6.4
0.625L	11.0						
0.70 L		10.3	10.7	10.0	9.1	9.7	8.5
0.75 L	11.5						
0.80 L		19.6	16.1	10.8	11.1	13.5	9.4
0.875L	17.7						
0.90 L		36.3	32.9	11.2	16.3	14.0	9.5
Crest	18.0	38.0	43.8	13.7	18.4	14.0	12.0

Table 5. Comparison of Measured and Calculated Values of the Velocity Distribution Exponent n.

Station	Run 217		Run 239	
	n (calculated)	n (measured)	n (calculated)	n (measured)
Crest	11.0	11.0	14.0	14.0
0.1 L	10.0	11.0	12.5	13.0
0.2 L	8.3	10.2	9.1	11.2
0.3 L	6.9	8.4	7.2	9.0
0.4 L	5.9	8.0	6.1	7.1
0.5 L	5.7	9.0	5.8	6.8
0.6 L	5.9	9.3	6.1	6.8
0.7 L	6.9	10.0	7.2	9.7
0.8 L	8.3	10.8	9.1	13.5
0.9 L	10.0	11.2	12.5	14.0
Crest	11.0	13.7	14.0	14.0